学位論文（要約）

Study on Nuclear Spin Manipulation in Single Quantum Dots by Optical Spin Pumping (Abridged)

(光スピン励起による単一量子ドットにおける核スピンの制御に関する研究)

平成29年12月博士（理学）申請

東京大学大学院理学系研究科

物理学専攻

Fong Chee Fai

フォン チーファイ

Study on Nuclear Spin Manipulation in Single Quantum Dots by Optical Spin Pumping (Abridged)

A Dissertation Submitted to
the Graduate School of the University of Tokyo
in Partial Fulfillment of
the Requirements for the Degree of
Doctor of Philosophy in Physics

by

Fong Chee Fai

December 18, 2017

Acknowledgment

First of all, I want to express my sincerest gratitude to my research supervisor, Professor Yasuhiko Arakawa, for giving me the great opportunity of joining the laboratory and agreeing to supervise this thesis. His knowledge, vision and ideas have always been a source of inspiration for me. Without his guidance, this thesis could not have been successfully completed.

I sincerely thank Prof. Satoshi Iwamoto. I remember our conversation on the first day I came to the lab. His support and encouragement have been an invaluable source of motivation and strength carrying me through my time here as a PhD student.

I am deeply indebted to Dr. Yasutomo Ota for teaching me more than just physics, for all the guidance, for giving me the room to grow as an independent researcher. I aspire to be to others what you have been to me as a mentor.

To Dr. Edmund Harbord who was instrumental to my pursuing of research of spin physics in quantum dots. He was there to help with my transition into the lab. From teaching me the basics of the experimental setup to continue mentoring me over internet calls, I simply cannot thank you enough.

I would like to thank Prof. Mark Holmes. Our many conversation about what research is has helped me deepened my understanding about the profession. It has also help me adjust my expectations about getting results and publishing, which in turn led to learn how to enjoy research.

I wish to express my thanks also to Dr. Evgeny Chekhovich, Dr Ata Ulhaq and Prof. Skolnick of the University of Sheffield. I had the opportunity to spend time at their lab as a summer student. While it was only a short 3 months, it proved to be an important part of my professional and personal growth, as it has helped me to learn to like research – skills leading to passion. In addition, I wish to thank Prof Akira Furusawa for his encouragement and concern throughout my time here.

My gratitude goes also to all the other members of the lab particularly to Kazuhiro Kuruma, with whom I had the pleasure of working with closely on studies with photonic crystals. To Dr Ryuichi Ohta and Dr Takumi Yamamoto who taught me about the setup and measurement techniques. Members of the lab, past and present, who contributed largely to the social aspect of my time here, thank you for making my PhD journey a joyous one. To Ms. Ritsuko Nara , Ms. Miwa Ouchi and Ms. Keiko Okumura, and, have helped me with various matters in lab, thank you very much. To those whose name I did not include here, I did not forget you all, I sincerely thank you.

Finally, I would like to thank my friends and my family, especially my parents without whom I would not be here.

Abstract

Semiconductor quantum dot (QD) nanostructures confine individual charge carriers in all three directions, leading to the formation of discrete energy levels, as such earning the moniker of "artificial atoms". QDs have attracted much attention over the last few decades for its potential in lasers, displays, telecommunications, spintronics, as well as for solid-state quantum computing technologies. QDs of III-V semiconductors, especially InAs and GaAs, are the most extensively investigated and thus have been at the forefront for realizing various applications. In particular for quantum computing technologies, the carrier spins trapped in QDs are suitable candidates as qubits and it has been predicted as well as demonstrated that these spins can have long lifetimes. However, as III-V materials have non-zero nuclear spins, the noisy environment from the fluctuation of the mesoscopic nuclear spins becomes a cause for concern as it is a prime source of carrier spin dephasing, which could significantly reduce the carrier spin lifetime. Just as the interaction between the nuclear and the carrier spins causes undesired loss of spin information, researchers have increasingly sought to make use of this interaction as a resource. The hyperfine interaction between the two spin systems allows for the transfer of spin from the carriers to the nuclei. As carrier spins can be optically oriented due to the selection rules of the interband transition, by continuous exciting spin polarized carriers in a QD, spin transfer could align the nuclear spins in a process known as dynamic nuclear spin polarization (DNP). The polarized nuclear spins cause a shift in the energy of the carriers, an effect that can be exploited to measure the degree of nuclear spin polarization.

This thesis presents the study on nuclear spin manipulation by optical spin pumping in single InAs/GaAs self-assembled QDs grown by molecular beam epitaxy. This thesis can be considered to consist of three main works.

In the first work, we showed the contribution to DNP by the first excited state (p-shell) electrons in a QD even at zero external magnetic field. DNP by these excited state electrons manifested itself in the observation of the increase in the degree of nuclear spin polarization along with increase of the excited state population. Furthermore, we measured the nuclear spin polarization time by employing a circular polarization modulation excitation. We observed

an abrupt increase in the length of time taken to polarize the nuclear spins, which we attributed to the suppression of nuclear spin decay due to the excited state electrons .

The second work focuses on the manipulation of the nuclear spin polarization by optical engineering using QDs embedded in photonic crystals. Photonic bandgaps are present in photonic crystals, resulting in modified density of states which in turn affects the radiative rate of the emission of the QDs. As DNP requires many repeated cycles of spin transfer, this process is thus limited by the radiative rate. By utilizing photonic crystals, we demonstrated the control of the degree of nuclear spin polarization by varying the radiative rate of QD emission.

We then outline a scheme for optical spin pumping for nuclear spin polarization by twisted light (light with non-zero orbital angular momentum). Due to the tight confinement of light in the cavity, the polarization (spin) and the spatial distribution of the light wave are no longer independently conserved, representing significant optical spin-orbit interaction. As a result, by exciting the cavity with a light beam with non-zero orbital angular momentum, we could generate spin polarized electrons in a QD which is coupled to the cavity. This spin polarized electrons can then polarize the nuclear spins.

The results presented in this thesis provide new insights on the dynamics of nuclear spin in QDs, as well as novel methods to manipulate the nuclear spin ensemble. These methods could be used together with previously reported schemes of electron spin qubit manipulation, for example, to alleviate electron spin dephasing, as well as paving the way for future devices such as nuclear spin based quantum memory and spin-photon interface for twisted light.

Contents

Chapter 1

Introduction

1.1 Research background

While spin is now understood as a quantum mechanical freedom with no classical counterpart, the concept was born before the formulation of quantum mechanics [1]. Fueled by observations of the "anomalous" Zeeman effect of atomic spectra, physicists sought for explanations which led to the proposal of a quantized electron degree of freedom. Following the publication of the seminal paper by Goudsmit and Uhlenbeck in 1925 [2], the idea of electron spin gained traction even among physicists who initially rejected the idea, most notably Pauli. Pauli then went on to propose a nuclear magnetic moment in order to explain the hyperfine structure of heavy atoms. This eventually led to the discovery that the proton, like an electron, has spin 1/2. Following the discovery of neutron by Chadwick, Heisenberg proposed that an atomic nucleus consist of protons and neutrons. The nuclear magnetic moment was then understood to arise from the proton and neutron spin. The concept of nuclear spin was thus born in the pursuit to understanding the atomic hyperfine structure.

About two decades after Goudsmit and Uhlenbeck's publication on electron spin, in pioneering work in metals carried out in the 1950s, Knight observed that polarized electrons lead to a shift in the nuclear magnetic resonance frequency [3] while Overhauser proposed to polarize the nuclear spins by transferring of spin polarization from electrons to the nuclear spins [4]. It would take another decade or so before the two fields of spin and semiconductor finally came together in 1968 with the first experiment on the optical spin orientation of electron to polarize the nuclear spins in bulk silicon performed by Georges Lampel [5]. While hardly an exhausting list, these three works mentioned here would have important implications on the study of spins in semiconductor nanostructures, to which we will come back in later paragraphs.

Advances in engineering inevitably led to the advent of semiconductor

nanostructures with the powerful ability to confine carriers – electrons and holes – at a quantum scale, making them structures with effectively reduced dimensionality. Particularly, semiconductor quantum dots (QDs), which provide confinement and quantization in all three spatial dimensions leading to discrete energy levels, has been of wide research interest. QDs have already been used to produce a range of devices including lasers [6] and liquid crystal display [7]. Furthermore, QDs hold the potential for future spin-based solid state quantum information technologies [8–13] with the electron (or hole) spin playing the role of a qubit.

The physical implementation of any quantum computing scheme should fulfill five main criteria as outlined by DiVincenzo [14] namely: 1) scalability of the qubits, 2) ability to initialize the qubit state, 3) long relevant decoherence time compared to gate operation times, 4) a "universal" set of quantum gates and 5) readout capability of qubit state. While significant progress has been made with QDs with regards to fulfilling these criteria, it is still an active field of research [15].

QDs has garnered much interest in large part due to the potentially very long spin lifetime[1] of the confined electron, which can in principle be of the order of milliseconds [16–19], a nod to criterion 3 in the previous paragraph. However, there are interactions which could reduce the spin lifetime. The interaction of an electron with phonons could be mediated by the spin-orbit interaction in a QD but unlike the case in bulk[2] or even 2D semiconductor, it was found to be less effective [21–24]. The spin-orbit interaction was even shown to be "tunable" electrically to achieve long spin lifetime [25]. On the other hand, confinement causes an enhanced hyperfine interaction, which is arguably the most significant source of the loss of spin information in a QD.

The hyperfine interaction is present in all III-V semiconductors[3] [28] as all the nuclear species have non-zero spin. A QD typical consists of $10^4 - 10^6$ atoms and thus an equally large number of nuclear spins which forms a mesoscopic system. The localization of the electron wave function around a

[1]Spin lifetime can be categorized into longitudinal spin relaxation time or spin lattice time, T_1 and transverse spin coherence time or spin-spin relaxation time, T_2. T_1 is the time for a spin polarized population of carriers to decay to a thermalized population via spin flip events. T_2 is a measure of the decay of quantum superposition of the spin states due to, for example, precession about a random, fluctuating magnetic field. The decoherence time of an ensemble of spin is usually referred to as T_2^*, also known as the dephasing time. There are also many instances where the terms "decoherence" and "dephasing" are used interchangeably.

[2]See reference [20] for a more detailed discussion of spin relaxation mechanisms in III-V semiconductors.

[3]Non III-V semiconductor QDs made of CdTe/ZnTe [26] and ZnO [27], for example, also have non-zero nuclear spins. The emphasis in the main text is on III-V systems as they are the most heavily studied and thus is most prevalent in the literature.

finite number of nuclei means that the electron spin interacts with a large number of nuclear spins leading to a strong hyperfine coupling [29]. These nuclear spin orientations are random and fluctuating, which could give rise to a small effective local magnetic field of the order of several milliTesla [30]. This effective magnetic field varies slowly enough such that it can be considered as a quasi-stationary "frozen" field on the timescale of the electron coherence ($\ll 1\mu s$) [31]. The electron spin precesses rapidly about this randomly oriented frozen field, leading to significant decoherence. The field is assumed to be random and has no preferred direction *i.e.* isotropic. The electron spin components which are transverse to the field will decay quickly, causing the electron spin polarization to fall to one-third of its initial value in a T_2 time of the order of a nanosecond. The effect of the frozen nuclear field on electron spin dephasing has been investigated in various QDs both optically [32–35] and electrically [16, 36].

A number of routes are being pursued to limit the dephasing by the fluctuating nuclear spins including the realignment of electron spins using the spin-echo technique [37–39], which has been shown to increase the electron T_2 time towards $1\mu s$. Besides electron spin, the hole spin has also been considered to store quantum information as it has a relatively weak hyperfine interaction due to its p-type atomic wavefunction [40–47].

It is also possible to alleviate the electron spin dephasing by applying a small external magnetic field to "screen" the fluctuation of the nuclear spin bath [32], however, this does not give a "true" narrowing of the nuclear spin distribution. Narrowing of fluctuation can be achieved by measurement and projection of the nuclear spin state [48–52] without necessarily polarizing the nuclear spin states.

Alternatively, one could polarize the nuclear spins [53, 54] in a process known as dynamic nuclear spin polarization (DNP). In fact, the hyperfine interaction itself facilitates the transfer of electron spin to the nuclear spin ensemble, a phenomenon now known as the Overhauser effect. Continuous optical [55–60] or electrical [61, 62] injection of spin-polarized electrons drives them away from the equilibrium spin polarization [20], giving rise to spin transfer which orients the nuclear spins along a certain direction (usually perpendicular to the sample plane). As the nuclear spin polarization decays on a much longer time scale relative to that of electron spin [63], DNP can generate a large effective nuclear magnetic field (also known as the Overhauser field) of up to several Tesla [62, 64, 65]. This Overhauser field in turn acts on the electron to shift its energy level and this is reflected in the splitting of the emission lines similar to that of the Zeeman effects (see chapter 3). As

such, the QD emission line allows us to study the dynamics of the coupled electron-nuclear spin system.

There are a number of spin flip mechanisms in the coupled electron-nuclear spin system. The dominant mechanism depends on the specific details of the experiments. In the case in strong magnetic fields and resonant excitation, the mutual spin flip-flop is inhibited by the large energy cost (due to the large difference in the Landé g-factors of electron and the nuclear species[4], electron-nuclear coupling mechanisms which does not involve simultaneous spin flips are dominant. The non-collinear hyperfine coupling, which arises from the nuclear quadrupole effects in QDs, is one such mechanism [66]. The spin flip from this coupling can induce nuclear spin relaxation under certain experimental conditions. For the case of non-resonant or quasi-resonant excitation where carriers are generated at energies above that of the transition of interest, with or without an external magnetic field, the mutual electron-nuclear spin flip-flop is the main spin flip mechanism. Essentially, an electron spin relaxes its initial orientation and the spin angular momentum gets transferred to the nuclei which could result in a net nuclear spin polarization [20].

It was assumed that a nonzero external magnetic field was necessary for DNP in QDs since the application of an external field of a few milliTesla to suppress the dipolar induced nuclear spin relaxation is a necessary experimental condition in the case of n-type bulk semiconductor [20]. However, Lai *et al.* demonstrated that significant nuclear spin polarization at zero external field was possible [67]. An explanation was proposed that the effective inhomogeneous magnetic (Knight) field generated by optically excited electrons is larger than the local nuclear field fluctuations, pre-empting the need for an external field. It was later suggested that the material strain-induced nuclear quadrupole interaction is more likely to be responsible for DNP at zero external field as the depolarization of the nuclei via the dipole-dipole interaction is supressed [68, 69].

The spin flip between the electron and the mesoscopic nuclear spin bath results in interesting nonlinear effects . One example is the observation of multiple nuclear spin configurations, of which two are stable and thus accessible via experiments. The non-Markovian nature of the dynamics leads to observation of the bistability of the nuclear field with respect to excitation power [64, 70–72], polarization of optical excitation [70] and external magnetic field [73, 74]. In these works, it was shown that the nuclear spin polarization

[4]In the case of Indium, taking an electron g-factor of 0.6, $g_e\mu_B/g_N\mu_N = 1000$, where $g_{e(N)}$ is the electron (nuclear) g-factor and $\mu_{B(N)}$ is the Bohr (nuclear) magneton. As such the electron spin states have a much larger separation compared to that of nuclear spin states.

can take a high or a low configuration depending not only on the experimental conditions but also the history of the experiment. The non-collinear hyperfine coupling is responsible for two other reported non-linear behaviours of emission line dragging effects where the QD resonance is "locked" to the resonant laser excitation and bidirectional DNP [52, 75, 76].

Nuclear spin polarization has led to more surprising observations such as the enhanced degree of spin polarization in charged excitons above the expected 1/3 of the initial polarization [59, 67, 77]. It has been proposed [53] and demonstrated that DNP can indeed lead to longer electron spin coherence time [78]. Complete nuclear spin polarization could in principle eliminate the electron spin decoherence effect, as well as enabling applications of nuclear spins as quantum memory [79–81]. Furthermore, high degree of nuclear spin polarization was also shown to be important for the generation of indistinguishable single photon [82]. Therefore, researchers have sought to achieve complete polarization of the nuclear spins.

However, there are a number of factors which limit the achievable degree of nuclear spin polarization via DNP. There is a low probability of electron-nuclear spin flip due to the large mismatch in the Zeeman splitting of electron and nuclear spins as mentioned in a previous paragraph. Furthermore, the mutual flip-flop mechanism of DNP requires many spin transfer from electron to nuclei meaning that the polarization of the ensemble of nuclei requires many cycles of excitation and deexcitation of carriers. Ideally, we would like to have fast removal of electron after spin transfer *i.e.* this process is limited by the exciton radiative lifetime [64], as well as the replacement of spin before loss of spin information and to avoid the depolarization of nuclear spins by the residual electron [73, 83]. Furthermore, the spin flip-flop probability is dependent on the interaction strength between the electron and nuclear spins which in turn depends on the overlap of their wavefunctions. This implies that DNP can be limited by the spatial extent of the electron wavefunction and thus becomes less and less efficient towards the "edge" of the electron wavefunction.

Nonetheless, there has been an upward trend in the highest reported degree of polarization in the last decade or so. The probability of spin flip-flop was shown to increase with temperature giving a degree of nuclear spin polarization of about 50% [84]. As temperature increase, the electron spin state broadens, enabling it to compensate for the energy mismatch of a larger number of nuclear spins and thus increasing the probability of spin transfer. Another approach succeeded in enhancing the efficiency of the spin exchange process by directly compensating the electron-nuclear Zeeman energy mismatch with

the energy of the photon via resonant optical excitation induced second-order (forbidden) processes, achieving ∼65% nuclear spin polarization [85].

It has been proposed that nuclear spins could form dark states which, if true, would not allow for complete nuclear spin polarization [54, 86, 87]. However, experimental verification of nuclear dark state is lacking. Recently, by combining optical excitation and advanced nuclear magnetic resonance technique, Chekhovich *et al.* has managed to achieve 80% nuclear spin polarization in a droplet etched GaAs/AlGaAs QD [88]. Ethier-Majcher *et al.* reported an electron T_2^* time of 39 ns, by way of nuclear spin state narrowing, alongside with a claim that this degree of narrowing is comparable to the effect of >99% nuclear spin polarization [89]. While the pursuit for complete nuclear spin polarization in QD is yet to conclude, these two recent works give much cause for optimism.

1.2 Research objective

In the thesis, we mainly explore novel methods to manipulate the nuclear spins in a self-assembled quantum dot via optical spin pumping. While previous works have made significant progress on studying various aspects about the nuclear spins, there remains a number of issues such as the complexity of the excitation scheme for nuclear spin manipulation and the need for the study of nuclear spins of QD in integrated devices, as well as the unexplored degree of freedom that can be exploited to control the nuclear spins, which we address in this thesis.

The reported approaches to manipulate the nuclear spins often involve rather complex excitation schemes dealing directly with the QD energy levels or states of excitons [52, 75, 85]. These schemes are often accompanied by high external magnetic fields of a few Tesla. In light of this, we seek a simpler alternative that enables DNP even with relatively conventional excitation and without any external magnetic field. This led us to our work on p-shell electron for nuclear spin polarization.

Besides external excitation, the nuclear spins and the mechanisms of DNP are inevitably affected by the physical properties of the QD sample such as the size, orientation and the presence of charge carriers, which could vary from QD to QD. While effort is being made towards more deterministic growth of QDs, we approach this issue by way of post sample growth processing – fabrication of photonic crystal – to manipulate the optical field and thus nuclear spins in the QD.

Optical excitation is one of the leading methods to introduce spin polarized

carriers into a QD which underpins DNP. Despite the recent advancement and prospect of optical excitation with non-zero orbital angular momentum (twisted light) [90], there is hitherto no conclusive experimental reports of such an excitation on a QD, most likely due small size of the QD [91] and the weak interaction of such excitation with the dipole transition in a QD [92, 93]. Nonetheless, not to be overlooked is the potential for using twisted light for optical spin pumping to polarize the nuclear spins in the QD. Orbital angular momentum could be an important degree of freedom present in the excitation that can be exploited to achieve higher degree of nuclear spin polarization.

In addition, the work presented in this thesis also serve to highlight the importance of studying nuclear spins of a QD embedded in a photonic crystal (PhC) as opposed to just a "bare QD". To realize a practical device with embedded QDs almost always requires integration with structures involving some form of postprocessing like micro/nanofabrication [94]. The fluctuating nuclear spins remain as a prime suspect for the source of electron spin dephasing in a QD-in-PhC system [95], however, it remains unknown if and how the embedding of QD in a PhC affects the nuclear spins. For example, the fluctuating surface charges (electrons) due to nanofabriocation could reduce the nuclear spin coherence of an embedded QD, which has not been studied. Therefore, it is imperative that we understand how a micro/nanostructure affects the nuclear spins in a QD and vice-versa if such a system were to be utilized as a device, be it a single photon source, a spin-photon interface or others.

The above-mentioned unresolved issues and prospects became the basis of the experimental and theoretical work described in this thesis.

1.3 Thesis outline

The current chapter gives an overview of the field of study, highlighting certain key results and issues. The rest of the thesis is structured as follows:

Chapter 2 describes the basic properties of semiconductor self-assembled quantum dots, which is the main workhorse. We describe its growth process and basic structure, as well as the resulting electronic and optical properties which in turn allows for the systematic investigations that we carry out.

Chapter 3 dives further into the details of the various spin systems in a self-assembled QDs, consisting of the electron, hole and nuclear spins. Here, we also describe the interactions between these different spin systems, outlining the underlying theories along with relevant equations.

Chapter 4 describes the work on DNP by p-shell electrons at zero external

magnetic field. We employed a laser excitation which modulates between right and left circular polarization, enabling us to extract the temporal information of the nuclear spin buildup even with a time-averaged detection. By measuring the power dependence of the nuclear spin buildup time we demonstrated the transfer of spin from p-shell electrons to the nuclei in a QD.

Chapter 5 focuses on the manipulation of the mechanism of DNP instead of dealing with the energy level of QD or the optical excitation. We looked at the underlying mechanisms of dynamic nuclear spin polarization which informed us that radiative lifetime is one of the limiting factors of the rate of transfer of electron spin to the nuclei. As such, by using photonic crystals which supports a photonic bandgap in which the density of state is suppressed and thus alter the emission radiative lifetime of the embedded QD, we showed how this in turn allows us to manipulate the resulting degree of nuclear spin polarization.

Chapter 6 describes a scheme for nuclear spin pumping in a QD with twisted light excitation. We explore how to utilize twisted light to manipulate the nuclear spin in QD by exploiting the functionalities of a photonic crystal nanocavity. Following from the optical spin-orbit interaction in the nanocavity, we describe how twisted light excitation could generate spin polarized carrriers in a QD which is coupled to the photonic crystal cavity. These carriers could then polarize the nuclear spins.

Chapter 7 summarizes the main contents as well as highlight the importance of certain aspects of this thesis. We also mention about the prospects and future work that could be done.

Chapter 2

Self-assembled Quantum Dots

There are many types of semiconductor quantum dots, usually categorized by their method of synthesis or fabrication, for example by molecular beam epitaxy (MBE), metalorganic chemical vapor deposition, colloidal chemistry, lithography or electrostatic potentials. The common feature of these QDs is their ability to confine electrons in all three dimensions, as such they are sometimes called "artificial atoms". The QDs studied in this work are self-assembled islands of a semiconductor embedded in another semiconductor of larger bandgap grown by MBE. Self-assembled QD tends to be smaller and can be easily integrated in device structures. QD have well confined optically active states with relatively large energy separation between the levels, making them attractive as emitters. This chapter gives an overview of the growth and the physics of these optically active systems. We briefly review the band structure of semiconductor which is relevant for our study on QDs. Then we discuss about excitonic complexes – bound states consisting of varied combinations of electron(s) and hole(s). Finally we discuss the optical selection rules that arise from the conservation of angular momentum associated with the bands.

2.1 Basic properties

2.1.1 Growth and quantum dot structure

A variety of III-V and II-VI strained material systems, like InAs/GaAs, InAs/InP, SiGe/Si or CdSe/ZnSe could give rise to the formation of QDs via the Stranski-Krastanov growth mechanism. In the epitaxial growth of these QDs, a substrate is heated and placed in ultra-high vacuum. Materials sources are heated which evaporates, giving off fluxes of atoms are then deposited layer by layer onto a substrate. Due to the lattice mismatch between the substrate and the deposited materials, a highly strained two dimensional wetting layer (WL) is formed on the surface of the substrate. At a certain critical thickness,

Figure 2.1: Schematic illustration of the QD growth process: InAs is deposited on a GaAs substrate forming a wetting layer. At a critical InAs thickness of 1.7ML, mechanical strain due to the lattice mismatch of the two semiconductor material leads to spontaneous formation of InAs island on the wetting layer. The QDs are annealed before capping with a GaAs layer.

a transition to island growth occurs. The formation of these islands is energetically favorable as the reduction of strain energy overwhelms the increase in surface energy and thus islands form spontaneously and randomly across the surface.

For the III-V InAs/GaAs material system, there is a 7% lattice mismatch between InAs and GaAs, giving a critical thickness of 1.7ML (monolayers) for InAs deposition on GaAs at 500^{o}C [96]. The critical thickness was found to increase with temperature [97]. The resulting lens-shaped QDs have a typical thickness of 3 – 5 nm and a diameter of about 20 nm. The density of the QD is typically determined by the substrate temperature and the amount of deposited In [98]. Following the growth of the QDs, a layer of GaAs is deposited over the QDs and this layer is usually known as the capping layer. During the deposition of this layer, the QDs are also subjected to annealing – when the QDs are partially covered by the GaAs capping layer, the sample temperature is temporarily increased, which results in the intermixing of Ga to the InAs QDs. This capping and intermixing reduces the height of the QDs to typically 1 – 2 nm [99, 100], blue shifting the QD emission energy to about 1.3 eV, convenient for use with conventional Si-based detectors in spectroscopic measurements. The optical properties of the QDs are highly dependent on the growth process, for example the fine structure described in Sec. 2.1.3 depends on the asymmetry of the shape, as well as the strain of the QDs. Also contaminants and residue from previous growth could lead to unintentional doping of the QDs with positive or negative charges.

2.1.2 Electronic properties and energy levels

The strain-driven island formation means that a QD consists of the order of 10^4 - 10^6 atoms. The overlap and hybridization of the valence electrons of these constituent atoms give rise to the electronic band structure. As InAs/GaAs QD are used for our study, our focus here will be on the III-V semiconductors.

The band structure of III-V semiconductors when considered with the effects of strain (Fig. 2.2) serves well to describe the case of these QDs.

Semiconductor GaAs and InAs have the zincblende structure. The conduction band (CB) is built from atomic s-type orbitals and thus it is doubly degenerate with a total angular momentum, $J = 1/2$ and values of the z-component of the total angular momentum, $J_z = \pm 1/2$. The parabolic dispersion of this band corresponds to the dispersion of a free particle with an effective mass, m_e^*. For GaAs and InAs, the typical values of effective CB electron mass are $m^*_{e,GaAs} \approx 0.063 m_e$ and $m^*_{e,InAs} \approx 0.023 m_e$ respectively where m_e is the free electron mass [101].

The valence band (VB), however, is built from atomic p-type orbitals with orbital angular momentum magnitude of one. Therefore, the structure of the band is subjected to the effects of spin-orbit interaction. As a result, the spin-orbit sub-band with total angular momentum $J = 1/2$ is split off by several hundred meV. Given the large splitting, transition involving the spin-orbit split-off band is usually not a concern during experiments. The remaining sub-band with $J = 3/2$ is 4-fold degenerate at the Γ-point but shows a different dispersion due to different $|J_z|$. The charge carriers in the $|J_z| = 3/2$ and $|J_z| = 1/2$ sub-band is referred to as heavy-holes (HH) and light holes (LH) respectively. The effective masses in GaAs are $m^*_{HH,GaAs} \approx 0.5 m_e$ and $m^*_{LH,GaAs} \approx 0.082 m_e$; in InAs are $m^*_{HH,InAs} \approx 0.41 m_e$ and $m^*_{LH,InAs} \approx 0.026 m_e$.

The band structure of a material is also altered by the presence of strain, which reduces the symmetry of the crystal and thus modifies the energy gaps and lifts degeneracies. In this case, the band structure can be treated using the Luttinger-Kohn Model. The HH and LH band energies can be calculated from the Luttinger Hamiltonian, while the effective masses of the bands are in turn given by the Luttinger Parameters.

In the case of a QD, both the confinement and strain can give rise to a splitting of HH and LH bands at the Γ point. The splitting Δ_{HH-LH} is typically of the order of 20 meV [102, 103], with the HH band being the top VB due to the compressive strain [20].

Under external excitation, for example the absorption of a photon by the QD, an electron in the VB can be promoted to the CB, leaving behind a hole. The 3D confinement of electron and hole is such that they can be described by single particle states occupying certain energy levels within the CB and VB respectively. The typical dimensions of a QD (e.g. 20 nm width and 2 nm height) suggest that confinement in the growth direction ($\hat{z}$) is typically strong. As such, following from the lens shape of the QD, the in-plane potential can

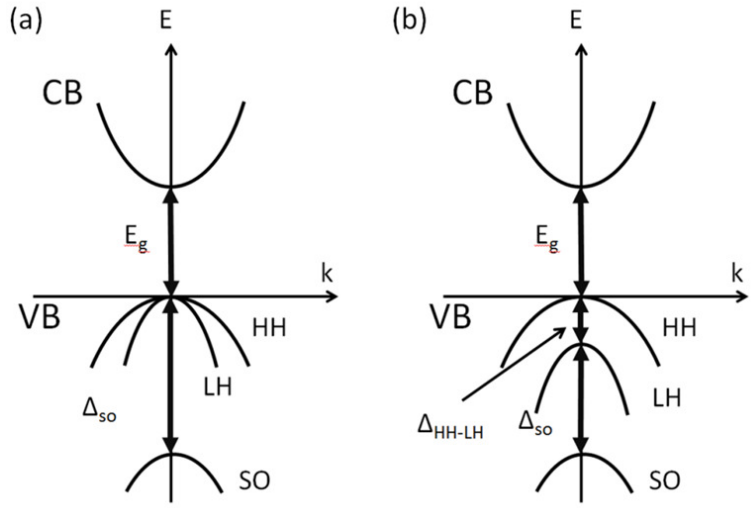

Figure 2.2: Scheme for the electronic band structure in the vicinity of the Γ point for a three-dimensional crystal with zincblende lattice structure (a) without strain (b) in the presence of uniaxial strain. The bands shown are the conduction band (CB), the heavy-hole (HH) band, the light-hole (LH) band, and the spin–orbit split-off (SO) band. E_g is the gap energy that separates the conduction and the VB. The band structure in (b) serves for the discussion of confined quantum dot states, where, in contrast to (a), the HH and the LH bands are split by Δ_{HH-LH}.

be approximated as a 2D harmonic oscillator while potential in the z-direction is treated as an infinite square well. The corresponding energy of the levels is then parameterized by the effective mass and confinement length, L^*: $E_n = \frac{\hbar^2\pi^2}{2m^*L^{*2}}n^2$, in addition to an offset in the energy due to confinement. The states are often referred to as "shells" with labels s, p, d and so on, which reflects the symmetry of the envelop wavefunction of these states in analogy to atomic orbitals (Fig. 2.3). As the effective mass of CB electrons is lower than that of VB holes, the level spacings for electron states are larger than that for holes states, on the order of 50 meV and 20 meV respectively.

2.1.3 Excitonic complexes

While energetically separated into two different bands, the confined electron and hole are spatially in close proximity. The Coulomb interaction therefore results in a bound electron-hole complex known as an exciton.

In the simplest case, there is an electron in the CB and a hole in the VB, forming a neutral exciton, X^0. There are 4 degenerate 1s excitons, that can be constructed from the electron spin ($\pm 1/2$) and heavy hole spin ($\pm 3/2$) states. These 4 possible excitonic ground states can be expressed in terms of the electron and hole spin states $|S_e, S_h\rangle$ namely $|+1/2, +3/2\rangle$, $|-1/2, +3/2\rangle$,

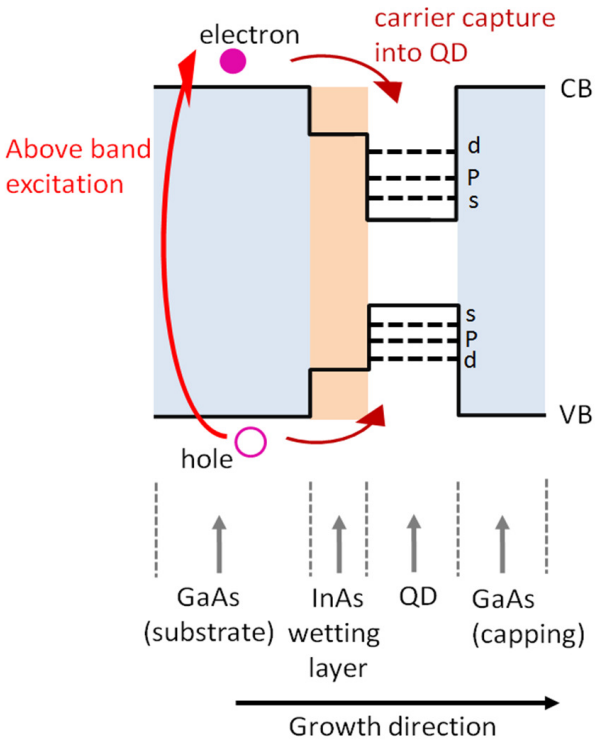

Figure 2.3: Schematic energy level diagram for an InAs QD embedded in GaAs along the growth direction. The discrete quantum levels are labelled in analogy with the atomic orbitals. Above band excitation, promotes an electron to the CB while leaving a hole in the VB, both which can then be captured into the QD.

$|+1/2,-3/2\rangle$ and $|-1/2,-3/2\rangle$. Alternatively, this may be characterized by the projection of total angular momentum onto the z-direction, M, as $|+2\rangle$, $|+1\rangle$, $|-1\rangle$ and $|-2\rangle$. States with $|M|=2$ are optically inactive (dark excitons) while states with $|M|=1$ are optically active (bright excitons).

However, the electron and hole spins can couple by the exchange interaction which is strongly enhanced in the case of the QD as compared to the case of bulk material. The strong confinement of the QD, together with the elongation of the QD along the $(11\bar{0})$ reduce its symmetry from $C_{4v}\rightarrow C_{2v}$, enhancing the anisotropic exchange interaction[1] (AEI). This AEI mixes the two degenerate $|\pm 1\rangle$ states into two non-degenerate states $1/\sqrt{2}\ (|+1\rangle \pm |-1\rangle)$ which are linearly polarized along the (110) and $(11\bar{0})$, also referred to as the major and minor axes of the QD respectively. These states are split by the anisotropic exchange energy, δ_{FS} (Fig. 2.4(a)). The dark states are split from the bright states by an exchange energy, while the dark states themselves are further

[1]AEI can be thought of as a mechanism which couples the electron and hole spins, enabling fast simultaneous relaxation. Alternatively, AEI can also be considered as an effective in-plane magnetic field. It is typically hundreds of μeV, much stronger than the effective frozen nuclear field. Thus, the frozen field has little effect on the spin dynamics of the electron in X^0.

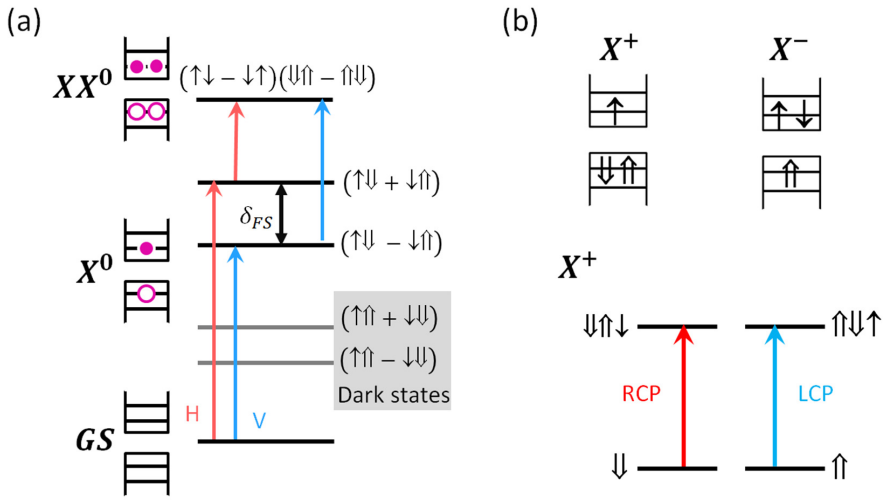

Figure 2.4: Schematic description of the energy levels and the configuration of (a) neutral and (b) charged excitons. $\uparrow$ ($\Downarrow$) represents an electron (hole) with spin up (down). For the neutral excitons, optical transitions are allowed between the ground state (GS) and bright states. Transitions are linearly polarized because of the mixed states. The bright states are split by δ_{FS}. The biexciton energy level exhibits no fine structure of it's own since the electrons and holes are paired in spin singlets. The fine structure of the biexciton arises due to its transition to exciton states. (b) Shown for the case of X^+, the ground state consists of a single hole spin and the transitions are circularly polarized.

split by the exchange interaction. The neutral biexciton, XX^0 consists of two electrons and two holes in spin singlets in the ground state. As the biexciton decay via either of the two routes (Fig. 2.4(a)) to form an exciton, the fine structure of the biexciton is identical but anti-correlated to that of the exciton. These mixed states emission can also be restored to their respective eigenstates by applying an external magnetic field which introduces a Zeeman splitting (see Sec. 3.1), in which case the transitions return from being linearly polarized to circularly polarized.

Extra "resident" carrier(s) can be introduced into the QD via doping (intentional or accidental) or by embedding the QD in a diode structure to enable charge tuning by the gate voltage. As the QD accepts carriers due to external excitation, the presence of the resident carrier will result in different exciton complexes. There are two types of singly charged excitons or trion complexes namely the positive trion, X^+ and negative trion, X^- (Fig. 2.4(b)). In its lowest energy state, the $X^{+(-)}$ consists of two holes (electrons) paired in spin singlet and an unpaired electron (hole). The Coulomb effect of these extra charges affects the emission energy and thus the charged excitons appear in the spectrum as distinct peaks from the neutral excitons. In these trion

complexes, the exchange interaction at zero field should vanish as an electron (hole) in $X^{+(-)}$ is interacting with a spin-singlet hole (electron) pair. The trion complexes have two degenerate excitonic states which couple radiatively to the light field with right and left circularly polarized emission respectively (shown for X^+ in Fig. 2.4(b)). The fine structure of charged excitons [104] are more complicated. For example, in the excited state, one of the carriers is in a p-like state (a hole for X^+ and an electron for X^-). In these cases, the exchange interaction comes back into play giving a non-vanishing fine structure, corresponding to different singlet and triplet states [105, 106].

Multiple excitonic complexes have been observed in single QDs. It is possible to generate biexcitons and charged biexcitons $XX^{\pm}$ by using higher excitation power [107, 108]. Even more highly charged states and their fine structure have been discussed [109].

2.2 Optical selection rules

Different excitonic complexes can have different carrier configurations and the spin of the exciton is determined by the sub-bands that the carriers occupy. The excitation of the carriers is governed by the selection rules which arise due to the conservation of angular momentum. These selection rules can be exploited to selectively excite spin-polarized electrons and holes into the CB and VB respectively. Optical transitions are possible from the heavy hole band, the light hole band and the split-off band. For the purposes of optical orientation, the energy of light is typically chosen to not excite carriers from the split-off band [20]. Figure 2.5 shows the transitions involving circularly polarized light from the heavy and light hole bands to the CB together with the relative transition strengths. Since the absorption of a circularly polarized photon must be accompanied by a change of angular momentum of magnitude one elsewhere, an electron–hole pair created by such an absorption can only take the paths as indicated in the figure. Right (left) circularly polarized, $\sigma(-)$, photo-generates spin-down (up) electrons and spin-up (down) holes, corresponding to a spin angular momentum of magnitude +1 (-1).

The degree of polarization can be defined as $DOP = \frac{I(\sigma+)-I(\sigma-)}{I(\sigma+)-I(\sigma-)}$, where $I(\sigma\pm)$ is the intensity of the $\sigma\pm$ circularly polarised light. In the case of bulk semiconductor (Fig. 2.5(b)), as the probabilities for the heavy hole transition is three times larger than that of the light hole transition, circularly polarized light that excites both transitions yields an ensemble of electrons with a maximum spin polarization of 50% [20]. In the case of QDs, as discussed in the previous section, quantum confinement lifts the heavy–light hole degeneracy.

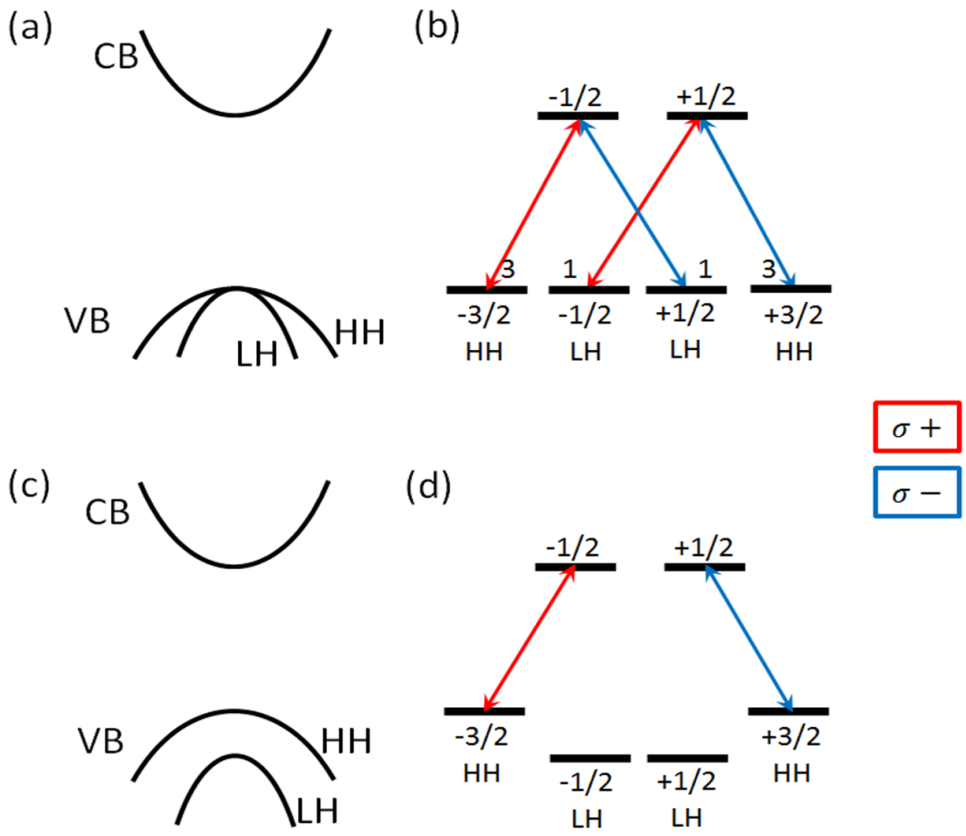

Figure 2.5: (a) Schematic illustration of bulk III-V band structure, (b) selection rules for interband transitions involving valence-band electrons for absorption and emission of circularly polarized light in bulk III-V semiconductor. The numbers by the arrows represent the relative transition strengths. (c) band structure of a confined or strained III-V nanostructure, (d) corresponding selection rules for absorption or emission of circularly polarized light in the nanostructure. A $\sigma+$ photon excites a $J_z{=}{-}3/2$ valence electron to the $J_z{=}{-}1/2$ CB and a heavy hole $J_z{=}{+}3/2$ is left behind in the VB.

In principle, the energy of the optical excitation may be tuned to only excite heavy holes whereby a 100% spin polarization may be achieved. However, quantum confinement also leads to population of states away from the Γ-point (i.e k $\neq$ 0), which induces an admixture of heavy and light hole states. As a result, the mixing partially allows nominally forbidden optical transitions, reducing the spin polarization of photo-generated electrons.

As the optical selection rules also apply in reverse, the circular polarization of the photon emitted from the QD in the growth direction will correlate with the spin of the recombining carriers. We could therefore measure the DOP of the QD emission to obtain insights about the spin polarization of electrons and holes.

Chapter 3

Spin Systems in a Self-assembled Quantum Dot

External optical excitation can generate carriers in the QD and the spins of these carriers can be oriented by controlling the polarization of the excitation. The carrier spind in the QD then interact with each other, as well as with the mesoscopic nuclear spin system. In this section, we will give an overview of the basic spin interactions of the QD electron, hole and nuclear spin, as well as discuss the various coupling mechanisms in these spin systems.

3.1 Carrier spin system

In a QD, the response of electron spins to an external magnetic field, $\mathbf{B_{ex}}$ is described by the Zeeman Hamiltonian

$$\hat{H}_z^e = g_e^* \mu_B \hat{\mathbf{S}}_\mathbf{e} \cdot \mathbf{B_{ex}}, \tag{3.1}$$

where g_e^* is the effective electron g-factor, $\mu_B = 58\ \mu$eV/T is the Bohr magneton and the spin operator, $\hat{\mathbf{S}}_\mathbf{e} = 1/2\ \hat{\sigma}$ with $\hat{\sigma}$ being the Pauli-matrices. This interaction will give an electron Zeeman splitting of $E_e^z = g_e^* \mu_B B_{ex}$. Similarly for holes, $\hat{H}_z^h = g_h^* \mu_B \hat{\mathbf{S}}_\mathbf{h} \cdot \mathbf{B_{ex}}$, where g_h^* is the effective hole g-factor and the hole spin operator is $\hat{\mathbf{S}}_\mathbf{h}$. In this form, the heavy hole spin is considered using pseudo spins of $\pm 1/2$ [110, 111] There is an analogous equation for the hole Zeeman splitting. In the case of an exciton, the exciton Zeeman splitting is $E_x^z = g_x^* \mu_B B_{ex}$, where the exciton g-factor, $g_x = g_e^* + g_h^*$.

3.2 Nuclear spin system

As for the nuclear ensemble containing i nuclear spins, the Zeeman Hamiltonian is given by

$$\hat{H}_z^n = -\sum_i \gamma_i \hbar \hat{\mathbf{I}}^i \cdot \mathbf{B_{ex}}. \tag{3.2}$$

Note that $\gamma_i \hbar = g_i \mu_i$ where g_i and μ_i are the nuclear g-factor and the nuclear magneton respectively. The gyromagnetic ratios for In and As are $\gamma_{In}^{115} = 9.37$ MHz/T and $\gamma_{As}^{75} = 7.32$ MHz/T.

In addition to the interaction with external magnetic field, nuclear spins interact with each other and usually the dominant interaction is the dipole-dipole coupling between two nuclear spins i and j. This interaction can be written as follows [112]

$$\hat{H}_{dip}^n = -\sum_{i<j} \frac{\mu_0 \hbar^2 \gamma_i \gamma_j}{4\pi r_{ij}^3} \left(\hat{\mathbf{I}}^i \cdot \hat{\mathbf{I}}^j - 3 \frac{(\hat{\mathbf{I}}^i \cdot \hat{\mathbf{r}}_{ij})(\hat{\mathbf{I}}^i \cdot \hat{\mathbf{r}}_{ij})}{r_{ij}^2} \right), \tag{3.3}$$

where μ_0 is the permeability of vacuum and $\mathbf{r}_{ij}$ is the vector of length r_{ij} joining the two nuclei. This Hamiltonian can be decomposed into "secular" part which commutes with $\hat{H}_z^n$ and "non-secular" part which does not commute with $\hat{H}_z^n$. The secular part is composed of terms which are proportional to $\hat{I}_z^i \hat{I}_z^j - \frac{1}{4}(\hat{I}_+^i \hat{I}_-^j + \hat{I}_-^i \hat{I}_+^j)$, where $\hat{I}_+^i$ and $\hat{I}_-^j$ are the raising and lowering operators of the i^{th} nuclear spin respectively. The secular part is therefore spin-conserving and responsible for nuclear spin diffusion within the lattice. The non-secular part, however, does not conserve the total angular momentum of the nuclear spin system[1]. The strength of the interaction $\hat{H}_{dip}^n$ is usually characterized by a "local field" B_l, which is the effective magnetic field generated on the site of a nucleus by its neighboring nuclear spins [112]. This local field can be thought of as the expectation value of Eq. (3.3) and for bulk GaAs, B_l is on the order of 0.1 mT [113].

Due to the large biaxial strain and intermixing of In and Ga in self-assembled QD, the cubic symmetry of the crystal breaks down, resulting in the presence of an electric quadrupolar moment which can couple to electric field gradients produced by electrons [114, 115]. Assuming axially symmetric electric field gradient *i.e.* uniaxial strain along the z-axis, the Hamiltonian can be expressed as [112, 116]

$$\hat{H}_Q = \frac{1}{2} \hbar \omega_Q \left(\hat{I}_z - \frac{I(I+1)}{3} \right), \tag{3.4}$$

[1]The non-secular part is responsible for the upper limit of the electron spin coherence time T_2 for a coupled electron-nuclear spin system [31].

where ω_Q is the quadrupolar angular frequency proportional to the z-component of the deformation tensor, e_{zz}. The quadrupole interaction can also be expressed as an effective field, $B_Q = \frac{\omega_Q}{\gamma} = \frac{\hbar\omega_Q}{g_N\mu_N}$, estimated to be of the order of 100 mT in self-assembled InAs QDs [68, 117]. The quadrupole interaction can lead to nuclear spin relaxation via its coupling to the modulation of electric field gradients arising from phonons or charge fluctuations in the QD [66, 118]. On the contrary, due the spatial inhomogeneity of the strain distribution, the quadrupole interaction causes neighboring nuclear spins to have different energy splittings which could in turn suppress the dipole-dipole interaction [69, 119]

3.3 Carrier-nuclear spin interaction

Optical selection rules dictate that circularly polarized excitation gives spin polarized electrons and holes. In the case of non-resonant excitation, the photogenerated carriers are accepted into the QD with capture time of the order of a few picoseconds [120, 121]. Both electrons and holes need to traverse through the quantum well-like wetting layer before being accepted into the QD. The hole spin experiences fast dephasing in the wetting layer resulting in spin lifetimes of the order of picoseconds [20, 122] which is comparable to the capture time. As such the hole spin is usually considered to be largely depolarized when it is captured into the QD. Furthermore, the hole spin and nuclear spin interaction is weak due to the p-like symmetry of the hole bloch wavefunction, resulting in negligible overlap with that of the nuclear spins.

The electron spin, on the other hand, has lifetime in a quantum well which is at least an order of magnitude larger than that of hole [20, 123, 124] and thus could retain its spin after being captured into the QD. Furthermore, the electron spin experiences strong interaction with the nuclear spins because of s-like symmetry of the conduction band Bloch wavefunction. Therefore, only the electron spin is considered to interact with the nuclear spins. The total Hamiltonian $\hat{H}$ for a single electron coupled to the mesoscopic nuclear spin ensemble can be written as [125]

$$\hat{H} = \hat{H}_z^e + \hat{H}_z^n + \hat{H}_{dip}^n + \hat{H}_{hf}, \tag{3.5}$$

where $\hat{H}_z^e$, $\hat{H}_z^n$ and $\hat{H}_{dip}^n$ are the electron Zeeman, nuclear Zeeman and nuclear dipole-dipole Hamiltonian, respectively. $\hat{H}_{hf}$ is the Hamiltonian for the hyperfine interaction, which couples the electron-nuclear spins.

In III-V semiconductors, the dominant contribution to the coupling be-

tween the confined electron and nuclear spin systems originates from the Fermi contact hyperfine interaction. This interaction can be written as

$$\hat{H}_{hf} = \frac{v_0}{2} \sum_i A_i |\psi(\mathbf{r}_i)|^2 \, \hat{\mathbf{S}}_e \cdot \hat{\mathbf{I}}^i, \tag{3.6}$$

where v_0 is the crystal unit cell volume containing two atoms, $\psi(\mathbf{r}_i)$ is the electron envelope wavefunction and $\mathbf{r}_i$ is the location of the ith nucleus. The hyperfine coupling constant, A_i is given by the equation $A_i = \frac{2}{3}\mu_0 g_0 \mu_B \hbar \gamma_i |u(\mathbf{r}_i)|^2$ where g_0 is the free electron g-factor and $u(\mathbf{r}_i)$ is the value of the electron Bloch function at the position of each nucleus. The values of A_i are as follow: $A_{In} = 56$ μeV, $A_{Ga} = 42$ μeV and $A_{As} = 46$ μeV [88, 113]. $\hat{\mathbf{S}}_e \cdot \hat{\mathbf{I}}^i$ can be written as $\hat{I}^i_z \hat{S}_z - \frac{1}{2}(\hat{I}^i_+ \hat{S}_- + \hat{I}^i_- \hat{S}_+)$, where $\hat{S}_+$ and $\hat{S}_-$ are the electron spin raising and lowering operators respectively. The first term on the right hand side is usually known as the static part which affects the energies of the electron and the nuclear spins. The second term with the raising and lowering operators is the dynamical part which is responsible for the transfer of angular momentum between the two spin systems via simultaneous spin flips. The contact hyperfine interaction can also induce an indirect dipolar coupling between spatially separated instead of neighboring nuclear spins, mediated by the electron spin, resulting in nuclear spin diffusion within the QD [126].

One can take the mean-field approach such that the static part of the hyperfine interaction leads to the notion of effective magnetic fields. The mean nuclear spin polarization gives rise to an effective nuclear field known as the Overhauser field, B_n while the spin polarized electron generates a Knight field, B_e. The corresponding Knight field operator $\hat{B}^i_e$ for the ith nuclear spin is given by

$$\hat{B}^i_e = -f_{el} \frac{v_0 A_i}{\hbar \gamma_i} \sum_i A_i |\psi(\mathbf{r}_i)|^2 \hat{S}_z. \tag{3.7}$$

The resulting Knight field, B^i_e depends on the electron spin state and on the location of the nucleus i. f_{el} is the fraction of time the QD is occupied by an electron or the relevant exciton containing a single electron responsible for generating a Knight field (and polarizing the nuclear spin). f_{el} is also known as the filling factor, taking a value between 0 and 1. The Knight field has been estimated from experiment to range from 0.6 – 3 mT for InAs/GaAs QD [60]. Similarly, the Overhauser field operator can be written as

$$\hat{B}_n = \frac{v_0 A_i}{g^*_e \mu_B} \sum_i A_i |\psi(\mathbf{r}_i)|^2 \hat{I}^i_z. \tag{3.8}$$

The generated Knight field has an opposite sign relative to the electron spin as

indicated by the minus sign in Eq. (3.7). Due to g_e^* which usually takes negative values, the resulting Overhauser field is thus aligned in the same direction as the electron spin. The Overhauser field leads to a shift in electronic states referred to as the Overhauser shift (OS), $E_{OS} = g_e^* \mu_B B_n$. In the presence of external magnetic fields, including the contribution of the OS, the total electron Zeeman splitting becomes

$$E_e^Z = g_e^* \mu_B (B_{ex} + B_n). \tag{3.9}$$

3.4 Dynamic nuclear spin polarization

The spin polarization of the electron is transferred to the nuclear spins via the hyperfine interaction, polarizing the nuclear spin ensemble. Under non-resonant excitation, the main mechanism of DNP is the mutual electron-nuclear spin flip-flop. This mechanism involves 3 basic steps, depending on the excitonic complex, the order of the events can be different. It is established that both positively charged exciton, X^+ (two holes and one electron) and negatively charged exciton, X^- (two electrons and one hole) couples strongly to the nuclear spin [58], therefore we will consider these two excitons here. In the case of X^+ (Fig. 3.1(a)) photogenerated carriers are first captured into the QD. The electron then exchanges spin with the nuclei, followed by radiative recombination with a hole to give a photon. For X^-, the last two steps are interchanged: an electron-hole pair recombines to leave a residual electron behind and then spin transfer from the electron to the nuclei takes place.The mechanism implies that, for both excitons, a shorter radiative lifetime will facilitate more spin transfers per unit time (Fig. 3.1(b, c)) when the injection rate is close to saturation.

In the absence of any other relaxation mechanism and the polarization of the electron or nuclear spins due to external magnetic field, the mean nuclear spin polarization $\langle I_z^i \rangle$ along the z quantization axis is given by [29]

$$\langle I_z^i \rangle = \frac{I^i(I^i+1)}{S(S+1)} \langle S_z \rangle, \tag{3.10}$$

where $\langle S_z \rangle$ is the mean electron spin along the z axis. In reality, the coupling of the nuclear spins to their environment depolarizes the nuclear spins, resulting in a nuclear spin configuration in a dynamic equilibrium. Therefore the mutual electron-nuclei spin flip-flop can be modeled based on the condition for dynamic equilibrium between the electron and the nuclear spin system. By including a nuclear spin decay channel characterized by time T_d, we obtain the

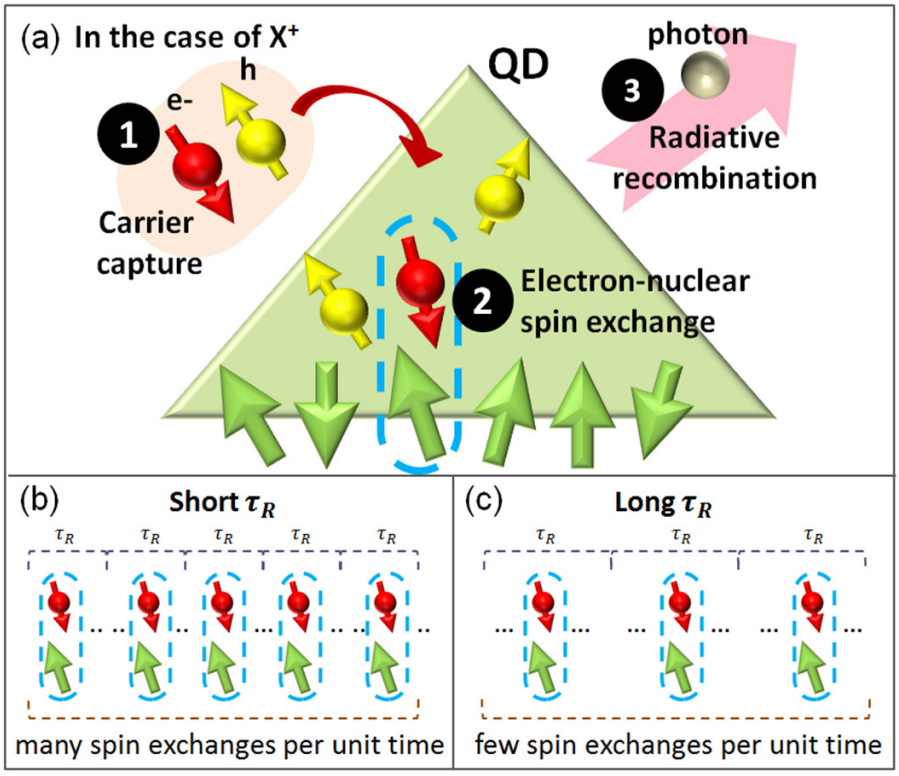

Figure 3.1: (a) Schematic figure showing the 3 basic steps involved in the process of DNP under non-resonant excitation with X^+ in a QD. In the case of short exciton lifetime (b), more spin exchanges between electron and nuclei can occur within a period of time than that of long lifetime (c).

following rate equation for the coupling of a single electron to a single nuclear spin [20, 112]

$$\frac{d\langle I_z^i\rangle}{dt} = -\frac{1}{T_{1e}}\left(\langle I_z^i\rangle - \frac{4}{3}I^i(I^i+1)\langle S_z\rangle\right) - \frac{1}{T_d}\langle I_z^i\rangle. \tag{3.11}$$

The first two terms on the right follows from equation 3.10 for $S = 1/2$. The nuclear spin exchange time[2] T_{1e} takes the form of

$$T_{1e} = T_{1e}^0\left[1 + \left(\frac{\tau_{el}}{\hbar}\right)^2 E_e^{Z^2}\right], \tag{3.12}$$

where τ_{el} is the electron-nuclear spin correlation time describing the broadening of the spin energy level $\hbar/\tau_{el}$. At zero total magnetic field, T_{1e} is simply $T_{1e}^0 = \left(\frac{N\hbar}{A_i}\right)^2/(f_{el}\tau_{el})$, where N is the number of nuclei. Depending on the experimental conditions, material and growth methods, T_{1e} could range from milliseconds [63] to seconds [72, 119].

Assuming a major contribution of nuclear spin diffusion from the dipole-

[2] T_{1e} is also referred to as the nuclear spin relaxation time as its formulation is based on the considerations of spin relaxation [29].

dipole interaction [26, 60, 127], T_d can be expressed as

$$\frac{1}{T_d} = \frac{1}{T_d^0} \frac{B_l^2}{(B_{ex} + B_e)^2 + B_l^2}, \tag{3.13}$$

where T_d^0 is the characteristic time of this interaction at zero field taken here as 0.1 ms, B_l is the local nuclear field as seen by each nuclear spin. A larger external field suppresses nuclear spin diffusion and thus increases T_d.

Equation 3.11 was obtained for the coupling of a single electron to a single nuclear spin. To approximately generalize it to the case of an ensemble of different nuclei in the QD, we consider the mean nuclear spin polarization, $\langle I_z \rangle = \frac{1}{N} \sum_i \langle I_z^i \rangle$. With this, we can replace the hyperfine constant A_i and the quantity $I^i(I^i + 1)$ each by a weighted average according to the relative compositions of In, Ga and As in the QD. For a realistic InAs/GaAs QD, the relative compositions is estimated to be $\rho_{In} = 0.3$, $\rho_{Ga} = 0.2$ and $\rho_{As} = 0.5$ [59, 115, 128]. Based on these values, we can take $A_i \approx 50$ μeV and $I^i(I^i + 1) \approx 13$.

Chapter 4

Dynamic Nuclear Spin Polarization by p-shell electrons

While the contribution of the first excited state (p-shell) electrons to DNP has been suggested in many previous work [129] it has not been studied so far. In this chapter, we describe the observation of p-shell carrier assisted DNP in single QDs at zero external magnetic field. The nuclear field continues to increase, even after the carrier population in the s-shell saturates. This is also accompanied by an abrupt increase in nuclear spin buildup time as p-shell emission overtakes that of the s-shell. We attribute the observations to p-shell electrons strongly altering the nuclear spin dynamics in the QD, supported by numerical simulation results based on the rate equation model of coupling between electron and nuclear spin system. DNP with p-shell carriers could open up avenues for further control to increase the degree of nuclear spin polarization in QDs.

4.1 Sample preparation and optical characteristics

To study the effects of carrier-nuclear spin transfers, we need to first identify the carrier types, *e.g.* excitons and/or shell. The sample under investigation was grown on a (001) GaAs substrate. A single InAs QD layer was capped with an 80-nm-thick GaAs layer. Atomic force microscopy analysis of uncapped samples gave an estimated QD areal density of about 5×10^8 cm^{-2}. This sample was subjected to rapid thermal annealing (annealing over a shorter period of time), tuning the recombination energy for a typical QD to around 1.3 eV at 10 K. Further details of the growth conditions can be found in ref. [130, 131]. The sample was patterned with 1 μm diameter mesas by e-beam lithography followed by dry etching, in order to perform single

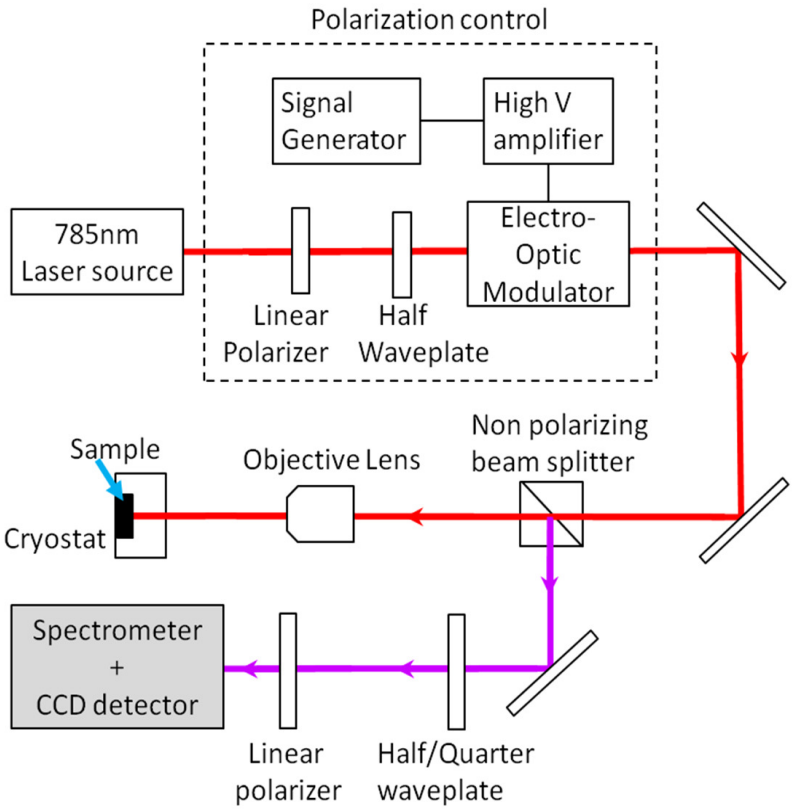

Figure 4.1: Schematic diagram of the micro-PL setup. Red (purple) arrows show the excitation (detection) path.

QD spectroscopy with a micro-photoluminescence (micro-PL) setup (Fig. 4.1). A continuous wave (CW) semiconductor laser operated at 785 nm is passed through a linear polarizer and a half waveplate to ensure that the polarization is in the right orientation for use with an electro-optic modulator (EOM). The EOM (Thorlabs EO-AM-NR-C2) consist of two crystals that exhibit the Pockels effect where the birefringence is proportional to the electric field. A signal generator is used to produce the required output waveform – DC or modulation – which is then fed into the high voltage amplifier before being supplied to the EOM. By applying the right voltages, the desired output polarization can be selected. The laser is focused on the sample with an objective lens (50×, NA = 0.65). The sample is held in a cryostat at a temperature of 7 K. The emitted PL is subsequently collected by the same objective lens and is analyzed with a computer controlled rotating quarter wave plate (QWP), followed by a linear polarizer, before being dispersed with a spectrometer and detected with a CCD. The linear polarizer is fixed and the QWP rotated, in order to avoid effects arising from the anisotropic polarization response of the spectrometer. Under non-resonant excitation, multiple emission peaks are observed in the PL spectra of QD. A typical PL spectrum is shown in Fig. 4.1(a). The peaks

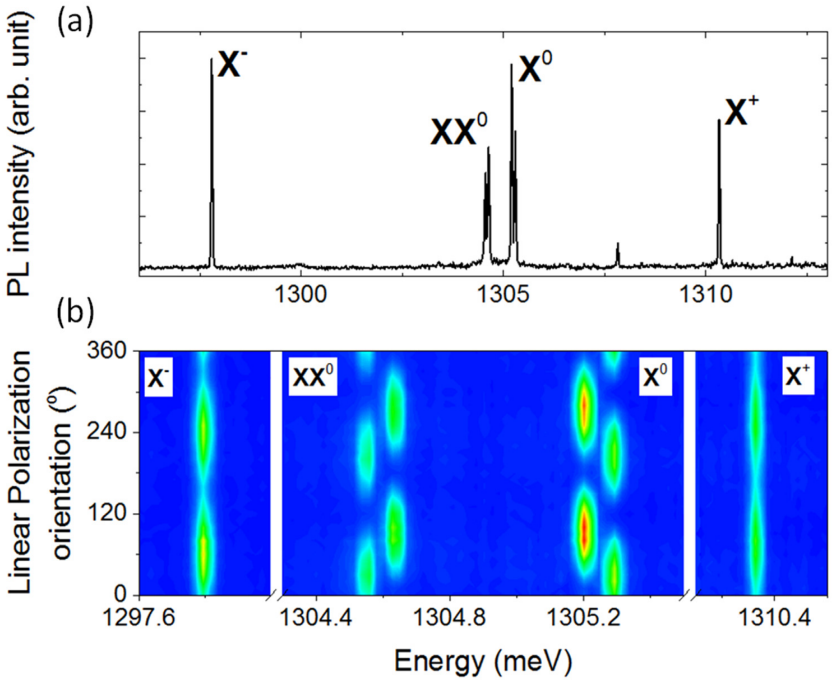

Figure 4.2: (a) A typical PL spectrum of the QD under investigation. (b) Color plot of the linear polarization dependence of the four main exciton peaks under linearly polarized excitation: charged excitons X^+ and X^- show no FSS in contrast with the neutral excitons X^0 and XX^0. Color plot is rescaled in the x-axis for clarity.

correspond to excitons and biexcitons, which can be distinguished by looking at the change in peak intensity with excitation power - in a log-log plot of intensity against excitation power, the gradient should be about 1 and 2 for excitons and biexcitons respectively [108]. Linear polarization dependent spectroscopy allows us to separate the neutral and charged excitons due to the presence (lack) of fine structure splitting in neutral (charged) exciton (see Sec. 2.1.3). To distinguish between positive and negative charged states, we performed optical orientation experiments where the QDs are pumped with circularly polarized light. As mentioned before, optical selection rules dictate that a maximum carrier degree of polarization of 50% can be introduced into the QDs, allowing us to generate spin majority carriers. The PL is detected at the two orthogonal circular polarizations using the QWP. The charged exciton at higher energy exhibited dominant co-polarized emission, allowing it to be unambiguously identified as X^+ [32, 132], while the lower energy peak is an X^- as it exhibits dominant cross-polarized emission [133, 134](Fig. 4.3(a, b)). This property is also reflected in the degree of polarization of the emission (Fig. 4.3(e, f)). For the case of X^+, $\sigma + (\sigma-)$ excitation will give positive (negative) DOP.

As excitation power increases, the rate of spin polarized carrier injection

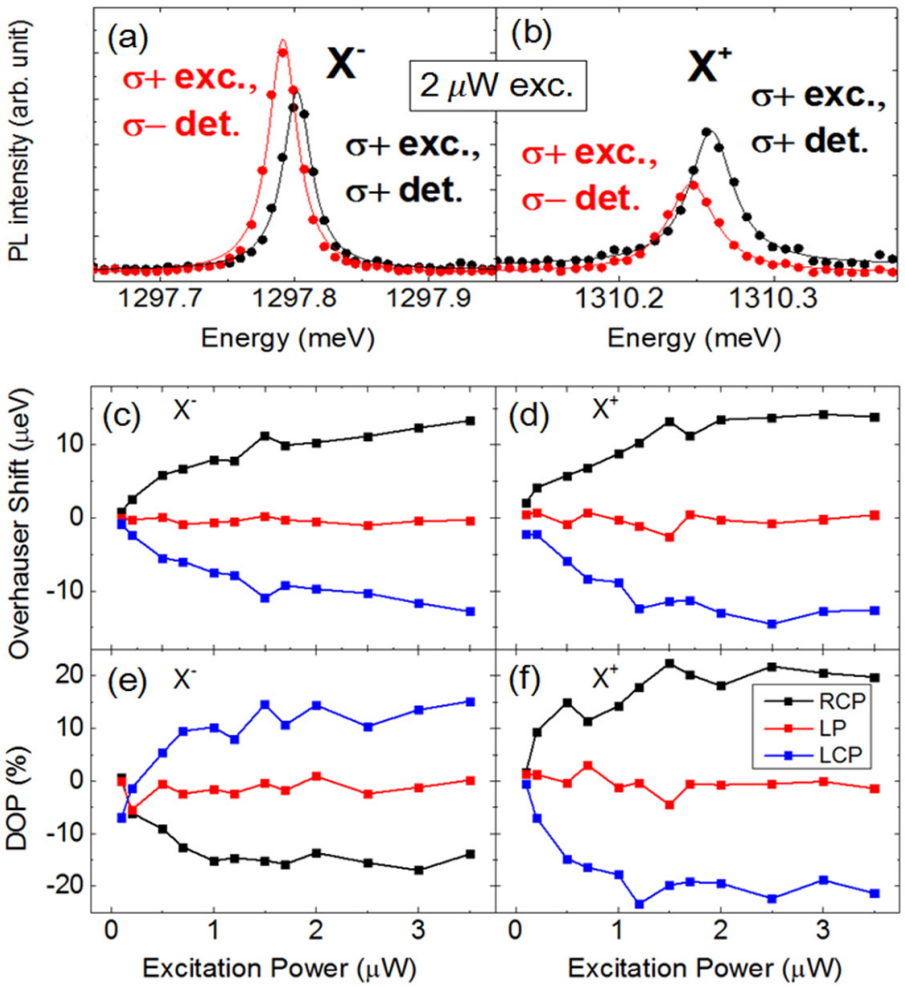

Figure 4.3: Top row shows the cross- and co-polarized nature of (a) X^- and (b) X^+ emission respectively. The separation between the peaks detected at orthogonal circular polarizations corresponds to the OS. Also plotted is the power dependence of OS and DOP of X^- (c, e) and X^+ (d, f) respectively under right (RCP, $\sigma+$), left (LCP, $\sigma-$) circular polarization and linear polarization (LP).

increases which in turn causes the OS and DOP to rise up to a certain value where the two quantities "saturates". At this stage, the rate of polarization of nuclear spin is equal to its rate of depolarization. X^+ and X^- exhibit very similar power dependence of OS and DOP suggesting that they contribute additively to nuclear spin polarization, consistent with previous report [135]. Under linearly polarized excitation, approximately equal amount of $\sigma\pm$ emission is generated, giving roughly zero OS and DOP.

4.2 Nuclear spin buildup time

Following the identification of emission peaks of QD, and their susceptibility to DNP, we investigated the nuclear spin buildup time, $\tau_{buildup}$, the QD is

excited with a laser beam which is modulated in σ^+ and σ^- polarization. By inputting a square-wave signal that alternates between the voltages for σ^+ and σ^- with frequency ω, a corresponding output is emitted from the EOM. The output laser beam is confirmed to be greater than 95% circularly polarized for both $\sigma^{\pm}$. The emission is collected over an integration time of 1 - 3 s in order to ensure that the QD is excited by a sufficient number of cycles of the polarization modulation to achieve dynamic equilibrium. The emission is detected at either one of the circular polarization.

Our proposed technique to investigate $\tau_{buildup}$ uses a fully time-averaged detection. As such, this technique is not limited by the detector speed which in turn allows for a simpler setup without the complicated excitation and detection control schemes. The high resolution of the spectrometer allows us to measure the OS of the exciton emission lines even at zero external magnetic field. Furthermore, the sensitivity of the OS coupled with the high spectral signal-to-noise ratio permits us to probe the modulation response over 4 orders of magnitude. As this is a spectrally resolved measurement, we can probe the shift of several different excitonic complexes within the QD simultaneously which is useful to identify the exciton which contributes to the nuclear spin polarization and to quantify the effect.

As the electron spin polarizes the nuclear spins in the same direction, alternating circularly polarized laser will generate B_n of alternating polarities. The $X^{\pm}$ emission peak consists of contribution from both σ^+ and σ^- excitation, each centered at a different energy separated by the OS. These contributions are not resolved since the OS is smaller than the linewidth of the emission peaks and thus giving a single peak with a larger overall linewidth. As such two Gaussian peaks are fitted to the spectra and the separation of the two peaks gives the OS (Fig. 4.4(a)). The key parameter in the two Gaussian fit is the width, which we obtain by measuring the linewidth under DC excitation at the same power and detection. In other words, the larger the full width at half maximum under polarization modulated excitation is compared to that under DC excitation, the larger the OS. While the areas of the two Gaussians should reflect the DOP (which can be determined from the DC excitation measurements), the areas of the Gaussians are set to be equal to simplify the fitting procedures. This was found to be of little consequence to the resulting OS and $\tau_{buildup}$ given the relatively low DOP – about 20% at saturation[1].

[1]By the selection rules, electron spin with 50% DOP could be achieved in principle. However, the electron spin experiences dephasing at the bulk GaAs, quantum well-like wetting layer before getting accepted into the QD. In the QD, the DOP further drops to 1/3 of the value when the electron gets accepted due to the fluctuating nuclear spins in about 1 ns, resulting in a DOP of <50/3 %. The observed DOP of ∼20% is a consequence of the back action of nuclear spin polarization, enhancing the DOP from its "expected" value

By extracting the OS for each modulation frequency, ω, Fig. 4.4(b) is obtained. The behavior of the OS vs ω can be considered to consist of three distinct regimes: at low modulation frequencies (< 0.1 kHz), the OS is at its maximum value. As the frequency is low compared with the $1/\tau_{buildup}$, the nuclei can follow the photo-modulated electron spin and the nuclei are polarized to the fullest extent possible under this degree of circular polarization. As the frequency increases, the measured OS reduces: each cycle of the modulation gets shorter and thus the nuclear spins get less polarized, resulting in weaker B_n and therefore smaller OS. At high frequencies (>10 kHz), the OS tends to a minimum indicating the absence of B_n. At these frequencies, the electron spins switch so rapidly that the nuclear spins do not get polarized.

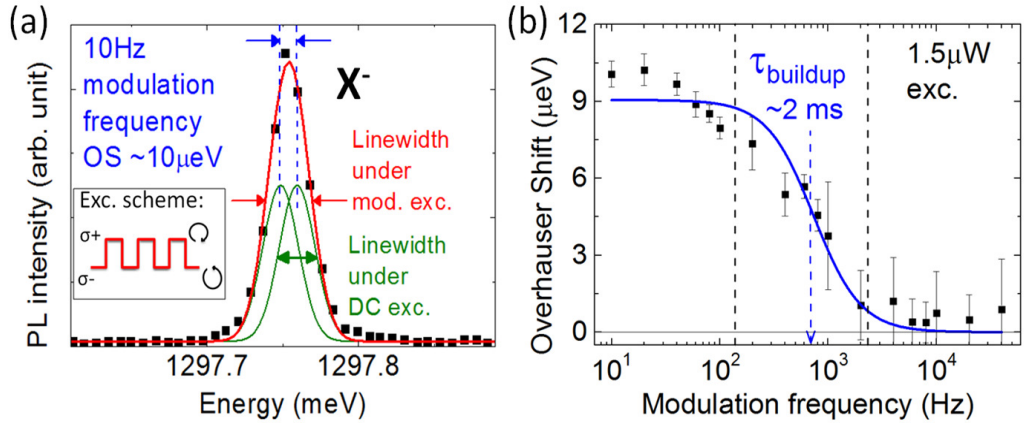

Figure 4.4: Spectrum showing a two Gaussian fitting (green solid lines) to an X^- peak where the separation of the fitted peaks give the OS. The red line gives the sum of the two fitted peaks. The respective linewidths under polarization modulation and DC excitation are as labelled. Inset shows the square wave circular polarization excitation scheme. (b) The change in OS with modulation frequency allows us to extract $\tau_{buildup}$ by fitting the data points with a Butterworth filter function. The dotted lines mark the three distinct regimes characteristic of such a measurement. The representative sample of data shown here indicates $\tau_{buildup}$ of about 2 ms at 1.5 μW excitation. The error bars represents the standard deviation of a number of data points taken at each frequency. The error in the value of OS could be induced by the instability of the position of the cryostat stage. The increasingly large error with modulation frequency is caused by the increasing uncertainty of the fitted peak position as the OS decreases.

Based on the rate equation for the optical pumping of nuclear spin (sec. 3.4), we solve for the square wave polarization modulation excitation with frequency ω, and obtained a solution in the form of the Butterworth filter function: $\langle I_z \rangle = \alpha / \left[\omega^2 + (\frac{1}{\tau_{buildup}})^2\right]$), where α is the amplitude fitting parameter to the

(c.f. sec. 1.1). The observed 20% DOP without an external magnetic field is consistent with other experimental reports [135]

spin polarization at no modulation (see sec. 4.4 for further details). By fitting this function to the data points, we could determine $\tau_{buildup}$. For the fitting process, we sometimes included a small constant offset in the fitting function in order to compensate for the fluctuation of the measured DC linewidths. The obtained $\tau_{buildup}$ is of the order of a few milliseconds, which is consistent to previous reported values [60, 63].

$\tau_{buildup}$ takes the form $\frac{1}{\tau_{buildup}} = \frac{1}{T_{1e}} + \frac{1}{T_d}$, where it depends on the relative magnitude of two underlying timescales, namely the nuclear spin polarization time, T_{1e} and nuclear spin decay time, T_d. In our experiments, the sample is under CW excitation and thus we can assume that the QD could be occupied with a residual electron for a significant amount of time, leading to fast nuclear spin decay such that $T_{1e} > T_d$. As such, $\tau_{buildup}$ is more susceptible to changes in T_d, which supports the results of the power dependence of $\tau_{buildup}$ in the following section.

4.3 P-shell assisted dynamic nuclear spin polarization

At high excitation power, in addition to the 4 main exciton peaks of the s-shell carrier recombination, the p-shell is also observed (Fig. 4.5). The energy separation of the p-shell from the s-shell emission is about 40 - 50 meV which corresponds to the separation in the energy levels in a QD, consistent with previously reported values [136]. A further confirmation of the p-shell emission is by looking at the PL power dependence which was observed to have the characteristic of super-linear increase [137]. The power dependence of the PL intensity of s- and p-shell emission (Fig. 4.6(a)) is measured by summing the integrated intensities of the peaks within 1297 – 1311 meV (1337 – 1352 meV) of Fig. 4.5 respectively. With increasing excitation power, the s-shell emission increases and then saturates, while the p-shell emission increases and eventually exceeds the s-shell emission intensity. In these high pumping-power conditions, the s-shell is closed and hence hinders the relaxation of p-shell carriers, which would otherwise relax to the ground state within a picosecond timescale [138, 139]. The prolonged lifetime of p-shell carriers increases not only the radiative recombination but also their interaction with nuclear spins.

Figure 4.6(b) shows pump power dependences of the OS and $\tau_{buildup}$. The OS curve shows a continuous increase, even after the saturation of the s-shell emission, and reaches an OS of more than 13 μeV without any external magnetic field. $\tau_{buildup}$ show a gradual increase at low pump powers, which could arise from an increase of T_{1e} due to suppressed electron-nuclear spin

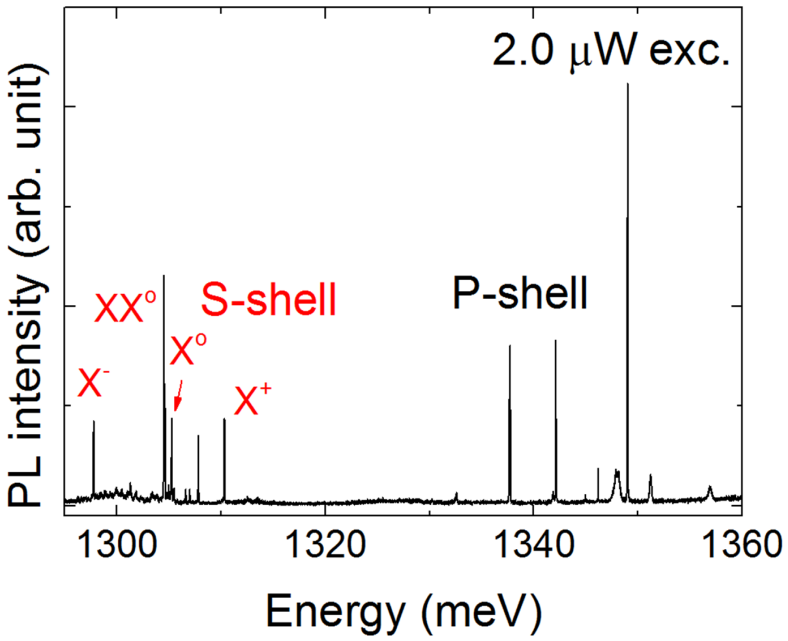

Figure 4.5: Under 2.0 μW excitation (without polarization modulation), p-shell emission can be seen clearly for this QD at energies about 50 meV higher than that of s-shell emission.

flip-flop processes by the increased nuclear field (which increases the energy mismatch between the electron spin states and hinders the flip-flop process). Then, $\tau_{buildup}$ shows an abrupt increase at excitation power above 1.5 μW, exactly when the p-shell begins to dominate.

The observed continuous increase of the OS along with a sudden jump in $\tau_{buildup}$ at high pump powers can be attributed to a slowed nuclear spin decay (increased T_d) and possibly hastened nuclear spin polarization (decreased T_{1e}). This is supported by numerical simulations (sec. 4.4) where we demonstrate that smaller T_{1e}/T_d ratios result in larger OS (c.f. eqn. 3.11): faster nuclear spin polarization and slower decay produce stronger nuclear fields.

The p-shell can support the suppression of the nuclear spin diffusion through the mechanism as explained below. A high spatial variation of p-shell electron wavefunction results in a strong inhomogeneity in the Knight field [119] inducing energy mismatch between neighboring nuclei (Fig. 4.7) and resulting in the suppression of nuclear spin diffusion through dipole-dipole interaction. The higher number of charged states of p-shell electrons and the greater degree of spatial variation of the p-shell could produce an even more strongly inhomogeneous Knight field. The inhomogeneous Knight field could lead to a quick rise in T_d and thus $\tau_{buildup}$. To rule out DNP by delocalized carriers in the wetting layer, we note that these carriers do not suppress the nuclear spin diffusion as reported in reference [119] and thus do not support the observation of the abrupt increase in $\tau_{buildup}$.

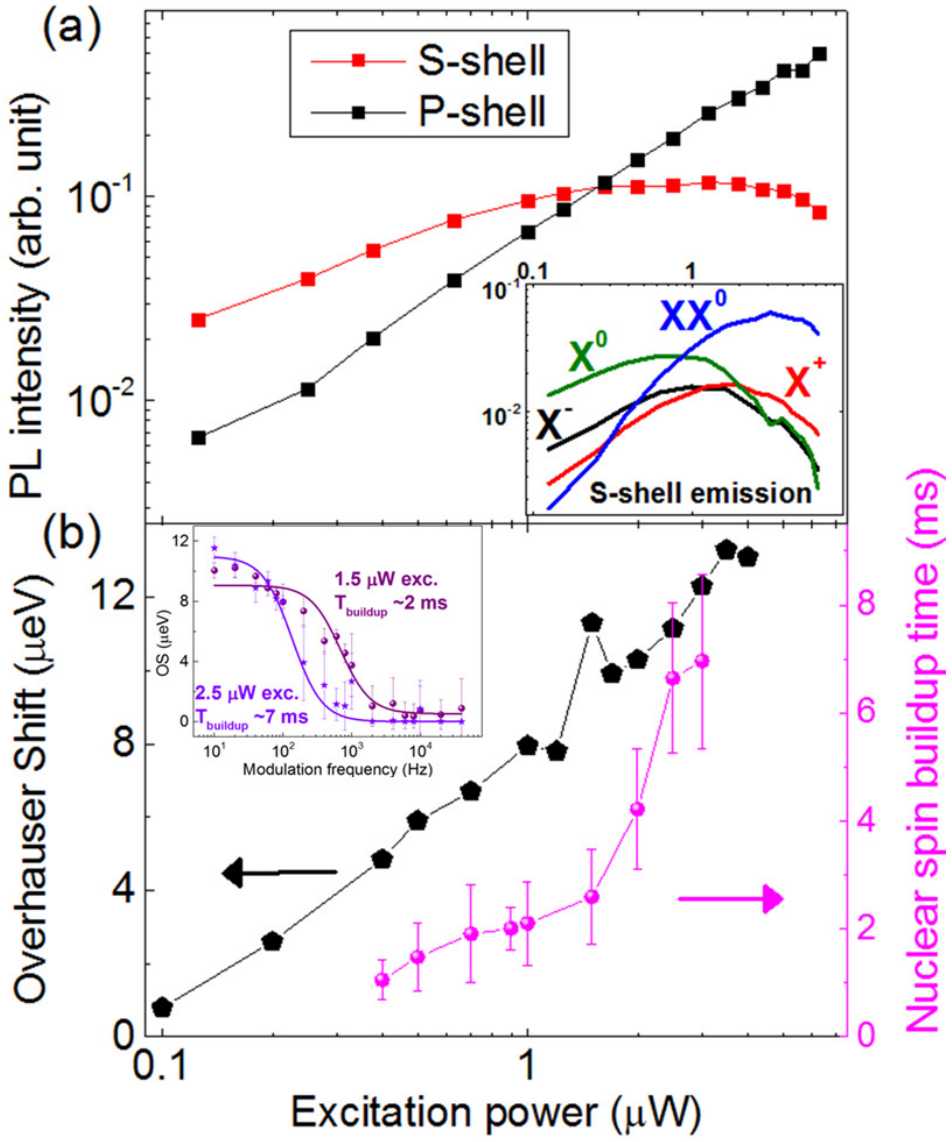

Figure 4.6: Plot showing the excitation power dependence of the s-shell and p-shell emission. The total PL intensity at each excitation power is obtained by summing the integrated intensities of peaks of s- and p-shell emission respectively. (Inset) shows the power dependence of four s-shell excitonic complexes. (b) The OS (black) under DC excitation increases with excitation power while the nuclear spin buildup time (magenta) remains relatively short before an abrupt increase as the p-shell state emission begins to overtake that of s-shell emission at just under 2 μW. The error bars of the buildup time are the standard deviation of a number of measurements at each excitation power. (Inset) Measurement of the change in OS of X^- with modulation frequency under two different excitation powers of 1.5 μW and 2.5 μW giving $\tau_{buildup}$ of about 2 and 7 ms respectively.

The p-shell could also contribute to nuclear spin polarization from two aspects. One is the increased probability to have unpaired electrons [136], which could translate to a larger number of states that could induce DNP. Another is a larger spatial extension of the electron wavefunction than that of

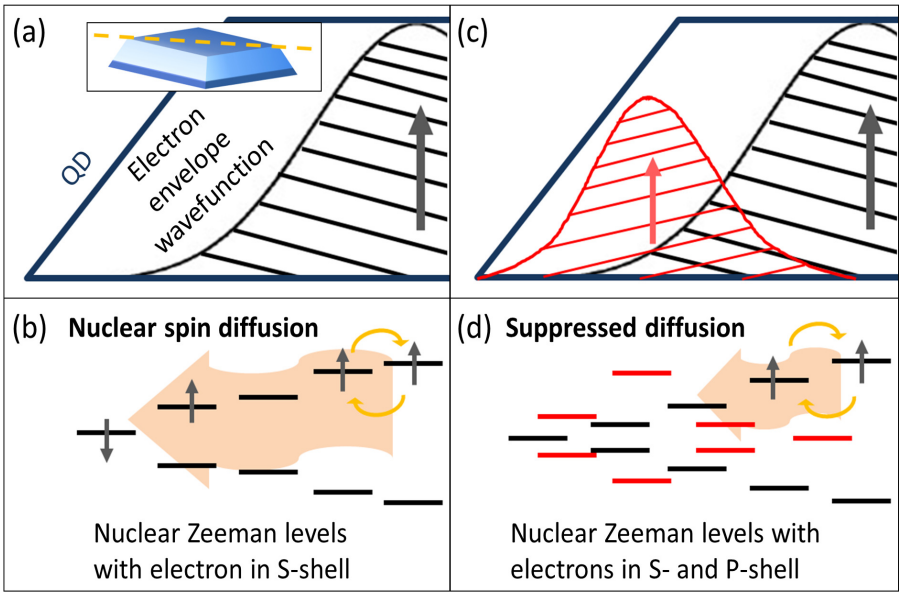

Figure 4.7: Schematic of the cross-section of a truncated pyramidal QD containing an s-electron (a) and the case with both an s- and p-electron (c). The inset in (a) shows the schematic of the truncated pyramidal QD. The cross-section is taken along the plane connecting the two vertices as indicated by the dashed yellow line. (b, d) Each electron generates a Knight field which in turn affects the nuclear Zeeman levels. Nuclear spins can undergo mutual spin flip with their neighbours via the dipole-dipole interaction and eventually diffuse out of the QD. This diffusion is suppressed when there are both s- and p-electrons in the QD.

s-shell, which assists the nuclear spin polarization in the exterior of the s-shell wavefunction.

We consider that the increase of T_d is predominantly responsible for the experimental observation. Although a decrease of T_{1e} can explain the increase of OS (since T_{1e}/T_d reduces), it cannot account for the increase of $\tau_{buildup}$ (given a fixed T_d). On the other hand, increase of T_d can consistently explain both the observations ($\tau_{buildup}$ jump together with the increase of OS) and is considered to be the more likely scenario. Indeed, numerically estimated T_{1e} is in excess of 30 ms, while T_d is less than 10 ms (see also Fig.4.10). As such any significant changes in OS and $\tau_{buildup}$ has to be due to changes in T_d.

We also rule out the possibility of a T_d increase solely due to the closing of s-shell. At high pump powers with dominant p-shell emission, the s-shell orbital tends to be filled with paired electrons which do not disturb nuclear spins and hence result in less nuclear spin depolarization and thus longer T_d. However, even at high pump powers, there remains significant emission from neutral/charged excitons of the s-shell (Fig. 4.6(a) inset) which consist of unpaired electrons that interact with the nuclear spins. Furthermore, the

residual electron after the recombination of X^- could facilitate depolarization. The combined effects of the polarization and depolarization by the s-shell excitonic complexes could at best give a small increase in T_d as the s-shell closes. Moreover, the closed s-shell cannot efficiently polarize the nuclear field and hence cannot account for the continuous increase of the OS. Overall, there is less likelihood of $\tau_{buildup}$ increasing along with continuous increase of the OS due to the closing of s-shell. Therefore we propose that changes of the nuclear spin dynamics arise, not from the changes in the s-shell but from the interaction between p-shell electrons and nuclear spins in the QD.

4.4 Modelling of nuclear spin response under circular polarization modulation excitation

To further support the abovementioned interpretation of nuclear spin dynamics, we carried out simulations using the rate equation described in Sec. 3.4. To model the $\sigma+/\sigma-$ polarization modulated square wave excitation, we introduced $\langle S_z\rangle = \langle S_z^0\rangle\, 4/\pi \sum_{n=1,odd}^{\infty} 1/n \left[\exp(in\omega t) - \exp(-in\omega t)\right]$. As DOP $= -2\,\langle S_z\rangle$ [84], the observed maximum DOP of 20% thus give $\langle S_z^0\rangle \approx 0.1$.

From equation of T_{1e}, the derivative of T_{1e} with respect to I_z shows that T_{1e} varies slowly with I_z. Therefore, ignoring the dependence of T_{1e} on I_z and solving Eq. (3.11) as a linear first order differential equation, the following steady state solution is obtained:

$$I_z(t) = \frac{16}{3}\frac{\overline{I^i(I^i+1)}}{nT_{1e}}\langle S_z^0\rangle \sum_{n=1,odd}^{\infty}\left(\frac{\frac{1}{nT}\sin(n\omega t) - \omega\cos(n\omega t)}{(1/T)^2 + (n\omega)^2}\right), \tag{4.1}$$

where $\frac{1}{T} = \frac{1}{T_{1e}} + \frac{1}{T_d}$. For B_{ex}=0, expressing OS $= g_e\mu_B B_N = 2\bar{A}_i\langle I_z\rangle$ [59], Eq. (4.1) becomes a self-consistent implicit time dependent equation for I_z. From the response part of the solution, we can see that it is in fact analogous to the Butterworth filter function. Following from this, we fit a simplified Butterworth filter function, $\langle I_z\rangle = \alpha/\left[\omega^2 + (\frac{1}{\tau_{buildup}})^2\right])$ to the data to obtain the buildup time. In addition to the above analysis with linear approximation, we performed numerical analysis of the non-linear form of Eq. (4.1) by including the dependence of T_{1e} on $\langle I_z\rangle$.

For each modulation frequency, I_z is first solved in the time domain for a time period corresponding to the integration time of the detector or alternatively over a few periods to reduce computation time. Figure 4.8 shows the temporal response of I_z under square wave circular polarization modulated excitation. Despite the discrepancy between the magnitudes of the nuclear spin

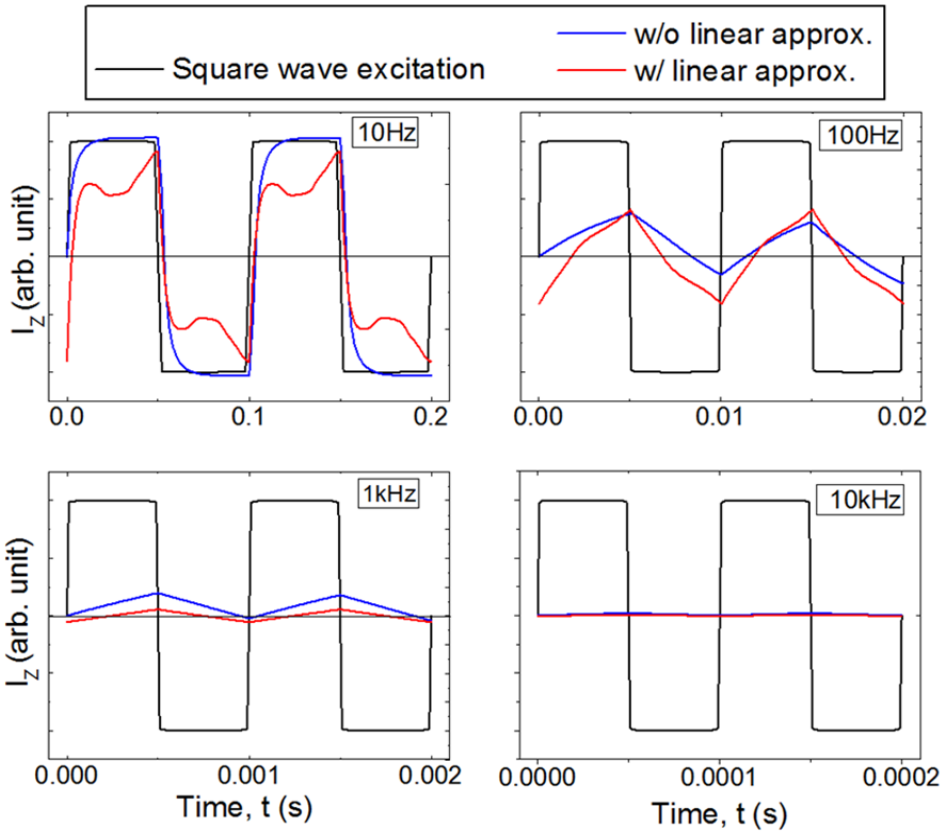

Figure 4.8: The temporal response of the nuclear spins is plotted against the square wave excitation (black lines) at modulation frequencies of 10 Hz, 100 Hz, 1 kHz, and 10 kHz. The red (blue) lines correspond to solutions with (without) linear approximation in Eq. (4.1). The two solutions are largely consistent with each other albeit the difference in the value of I_z. As the modulation frequency increases the modulation amplitude of the nuclear spin polarization decreases as observed in the experiments.

polarization for the solutions with and without linear approximation, both gave similar modulation of the nuclear spin polarization with the excitation. The overall behaviour where the nuclear spin polarization decreases with increasing modulation frequency can be clearly seen in the temporal behaviour.

To obtain the time average value of I_z i.e. $\langle I_z \rangle$ for each modulation frequency, the mean of the absolute value of I_z in the time domain is calculated (the mean values would be effectively zero as I_z oscillates between positive and negative values). The mean of the absolute value is taken as $\langle I_z \rangle$ in this case since the double Gaussian fitting does not distinguish the direction of the OS. Simulation results of the change of OS with modulation frequency is consistent with that from experiments, allowing us to conclude that the linearization assumption is valid, so are the analytical solutions of $I_z(t)$ and $\tau_{buildup}$

For a fixed value of $T_{1e}^0 = 40$ ms, Fig. 4.9 shows how the nuclear spin polarization response to modulation frequency changes for different values of

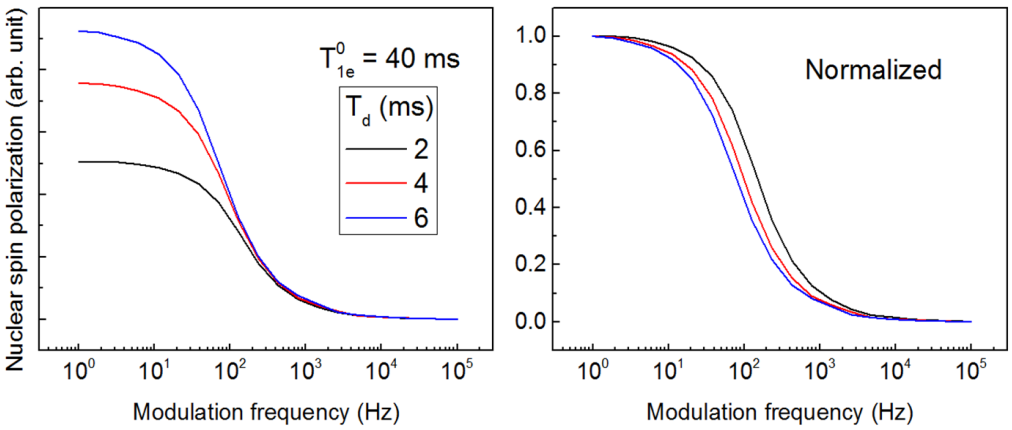

Figure 4.9: The plots show the change of the nuclear spin polarization with modulation for T_d = 2, 4 and 6 ms without linear approximation. Other parameters are fixed at T_{1e}^0 = 40 ms and τ_{el} = 60 ps. As T_d increases (ratio T_{1e}^0/T_d decreases) nuclear spin polarization starts to decrease at lower modulation frequency, meaning longer $\tau_{buildup}$.

T_d. For longer T_d, there is less nuclear spin diffusion per unit time and thus the maximum achievable nuclear spin polarization at low modulation frequency is higher. The normalized plots show how the nuclear spin polarization starts to decrease at lower frequency for longer buildup times and vice versa.

Figure 4.10 shows a series of simulated OS as a function of T_{1e}^0 and T_d under three different τ_{el} (all other parameters are fixed). It is apparent that the maximum OS essentially depends on the ratio T_{1e}^0/T_d. A small ratio reflects a high rate of polarization to decay and thus giving large OS while a large ratio gives the opposite. The resultant OS is also dependent on the electron correlation time, τ_{el}. Increasing τ_{el} narrows the energy broadening which in turn decreases the probability of spin flips and therefore lowers the resulting nuclear spin polarization. However, regardless of the value of τ_{el}, the regions which span the observed OS in the experiment indicates that $T_{1e}^0 > T_d$ as expected.

Matching the experimentally-observed OS to the simulation results, OS of 1 μeV to 13 μeV corresponds to T_{1e}^0 between 40 ms to 120 ms, while T_d ranges from 2 ms to 6 ms, or possibly larger for both timescales. It is worth noting that unlike T_{1e}^0, T_{1e} is magnetic field dependent such that with any magnetic field (in our case, nuclear field B_n), the value of T_{1e} is always greater than T_{1e}^0. Given the relatively large T_{1e}, its reciprocal should remain relatively constant, therefore leaving $\tau_{buildup}$ to be easily affected by the increase in T_d, supporting experimental observation.

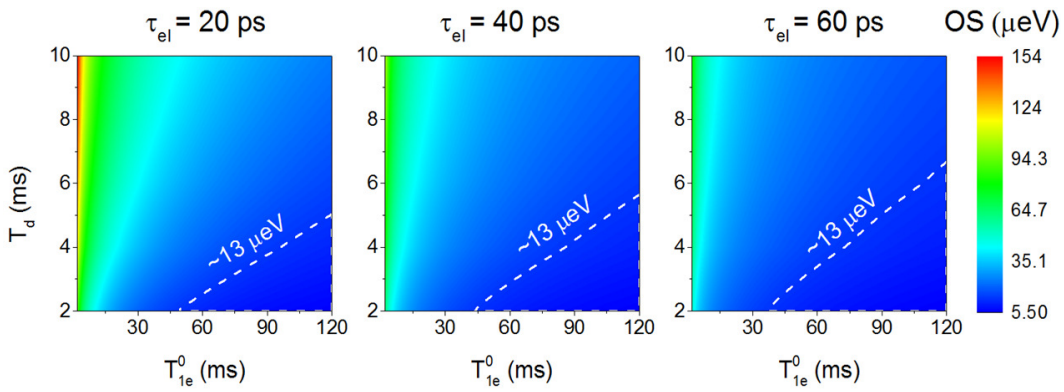

Figure 4.10: Color plot of the maximum OS obtained over a range of T_{1e}^0 and T_d values for τ_{el} = 20, 40 and 60 ps. Systems with short spin flip time and long nuclear spin decay time will give high OS corresponding to the top left corner of each plot. For higher values of τ_{el}, the spin flip probability decreases and thus for the same values of T_{1e}^0 and T_d, the achievable $\langle I_z \rangle$ is less. The dashed line marks the approximate maximum OS observed in the experiments indicating that we are essentially operating in the regime where $T_{1e}^0 > T_d$.

4.5 Summary

We observed p-shell assisted DNP in QD at zero external magnetic field. We observed continued increase of the OS and a jump in $\tau_{buildup}$ as the p-shell emission becomes dominant. It was found that p-shell carriers are responsible for the increase in nuclear spin polarization after the saturation of the s-shell. The contribution of p-shell electrons to DNP is supported by measuring the power dependence of the nuclear spin buildup time. We consider that p-shell electrons slow down the nuclear spin diffusion by increasing the inhomogeneity of the Knight field. These in turn led to a continuous increase of OS after closing the s-shell together with the marked increase in the nuclear spin buildup time.

We presented a technique which uses time-averaged measurements to investigate the nuclear spin buildup time via polarization modulated excitation. Despite the various simplifying assumptions in the semi-classical model we have validated the technique by comparing experimental results with simulations, both resulting in nuclear spin buildup times of the order of milliseconds, consistent with previously reported values. The buildup time is governed by the T_{1e}^0 parameter which is consistent with the phenomenological modelling in reference [60].

The use of the p-shell also enables more nuclear spin polarization due to increased electron-nuclear spin interaction. Control over the population of the p-shell could allow us to break the current limit in nuclear spin polarization.

Chapter 5

Control of Dynamic Nuclear Spin Polarization by Vacuum Field Engineering

Optical spin pumping into QD embedded in a photonic nanostructure represents an important step towards quantum computing technologies, which utilize the carrier spin as a qubit resource. In addition to being able to facilitate generation of spin polarized carriers, photonic nanostructures also allow us to manipulate the local spin environment of a QD including the nuclear spins. In this chapter, we describe experiments to manipulate the dynamic nuclear spin polarization by engineering of the photonic environment using 2D air-hole photonic crystals (PhC). We find that the achievable degree of nuclear spin polarization can be controlled through the modification of exciton radiative lifetime due to the photonic bandgap effect. We find a tendency where the increase in radiative lifetime, results in lower degree of nuclear spin polarization.

5.1 Sample and experiment details

The sample consists of a single layer of InAs/GaAs QD embedded within a lithographically defined PhCs (lattice constant of 250 nm, triangular lattice with air hole radius of 72.5 nm, air bridge structure with 130 nm slab thickness) (Fig. 5.2(a)(inset)). The embedded QD has a density of about 1.0×10^8 cm^{-2}, emitting mostly between 920 nm and 950 nm. This emission band is well within the simulated photonic bandgap, in which the photonic density of state is significantly reduced and hence the QD radiative emission rate $1/\tau_R$ as described by the Kleppner effect[140]. Detailed description of the PhC fabrication can be found in reference [141].

The sample was set in a cryostat at 7 K and was investigated using a micro-

PL setup. A continuous wave semiconductor laser operated at 785 nm was focused on the sample with an objective lens (50×, NA = 0.65). The emitted PL was subsequently collected by the same objective lens and was analyzed with polarization detection optical components where relevant, before being dispersed with a spectrometer and detected with a CCD. To measure the QD emission radiative lifetime τ_R, a linearly polarized semiconductor pulsed laser (PicoQuant) with an emission peak at 785 nm and ∼50 ps pulse length, was used together with an avalanche photodiode detector with an estimated resolution (instrument response) of 400 ps. External magnetic field was applied using permanent magnets - a ring magnet placed on top of the cryostat to give 0.07 T and a flat cylindrical magnet placed directly underneath the sample inside the cryostat to give 0.15 T in the Faraday geometry (Fig. 5.1). The magnetic field strength was first measured using a magnetometer over a range of distances and positions from the magnets in order to determine the field strength at the position of the QD sample.

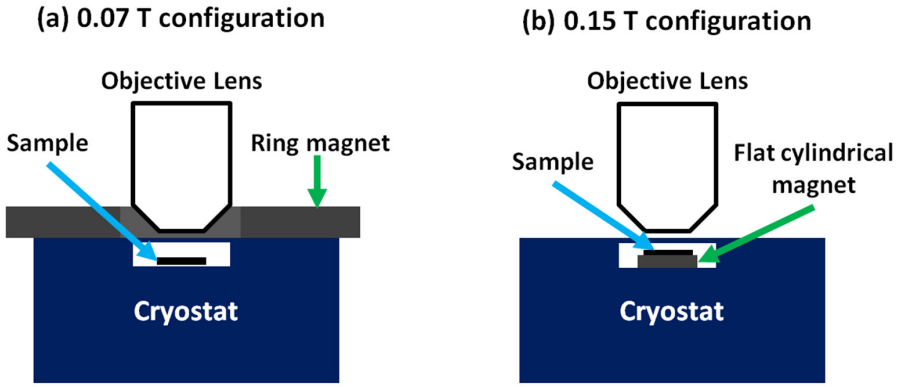

Figure 5.1: Different configurations are used to generate the external magnetic field around the QD sample: (a) a ring magnet placed on top of the cryostat for 0.07 T and a flat cylindrical magnet placed underneath the sample inside the cryostat for 0.15 T.

Micro-PL spectroscopy was carried out on bare QDs (outside of PhC) and QDs in PhC on the same sample.We focus on X^+ given that it is the dominant exciton observed in our QD-in-PhC sample (Fig. 5.2). Basic characterization such as power dependence and polarization dependence of the emission was first carried out to determine QD with X^+ (see also Sec. 4.1). The excitation power was chosen to be sufficiently high such that the carrier injection rate is high, giving maximum X^+ emission intensity, in order to maximize the achievable degree of nuclear spin polarization. In this case, the radiative rate is limited by the radiative lifetime. As X^+ is the dominant exciton in the QDs, it is the main contributor to the nuclear spin polarization and thus maximizing X^+ emission will bring the OS to saturation or close to saturation. Given the

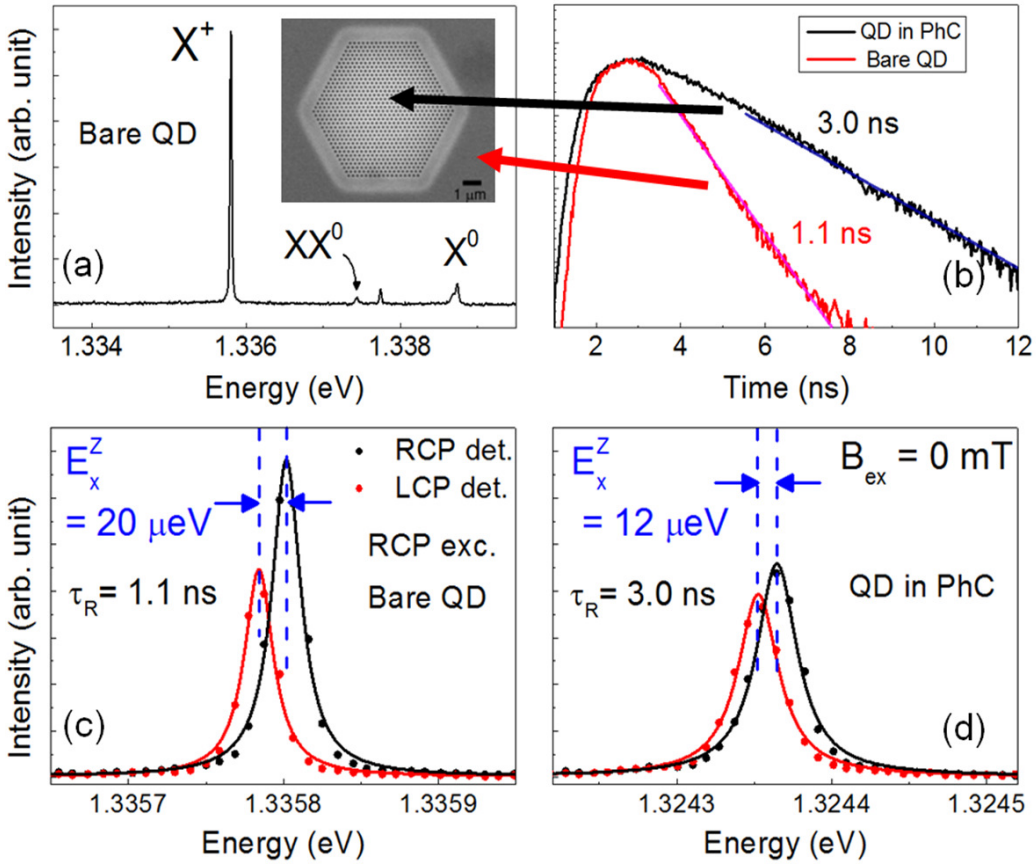

Figure 5.2: PL spectrum of the bare QD showing dominant X^+ emission. (Inset) Scanning electron micrograph of a 2D PhC embedded with QD. (b) Exemplary time-resolved measurements comparing a bare QD and a QD in PhC giving 1.1 ns and 3.0 ns radiative lifetime respectively. The dark blue and magenta lines indicate fit to the measurement to extract the radiative lifetime. The arrows indicate the area on the sample where the two types of QDs can be found. (c, d) Plots showing the corresponding Zeeman splitting obtained for bare QD and QD in PhC under RCP excitation at $B_{ex} = 0$ T, giving 20 and 12 μeV respectively. The relative peak intensity under RCP and LCP detection shows co-polarized emission as expected of X^+. The large (small) magnitude of DOP for bare QD (QD in PhC) is in accordance to the respective radiative lifetimes. Under LCP excitation (not shown), nuclear field of opposite direction is generated and thus the Zeeman splitting takes the opposite sign compared to that under RCP excitation.

low external magnetic field in the experiments, neutral excitons, multiexcitons or other excited state process are not expected to have significant contribution to nuclear spin polarization [142]. The polarization of the emitted photon is mainly determined by the spin polarization of the electron before radiative recombination. Nuclear spin polarization could also screen its own fluctuations and thus reduce spin decoherence, as such the degree of polarization (DOP) of emission can give insights about the nuclear spin polarization. Therefore for each QD, we measured τ_R, Zeeman splitting. E_x^Z and DOP.

An exemplary measurement of intensity decay curves of a bare QD and a QD in PhC at zero external magnetic field is shown in Fig. 5.2(b). By performing a linear fitting to the exponential decay curve, τ_R can be extracted. In this example, the QD in PhC shows longer τ_R of about 3 ns, almost 3 times longer than the 1 ns of the typical bare QD. Consequently, lower E_x^Z and DOP was observed for QD in PhC ($E_x^Z = 12$ μeV, DOP = 30%) than for bare QD ($E_x^Z = 20$ μeV, DOP = 15%).

5.2 Nuclear spin polarization with photonic bandgap effect

We repeated these measurements for many single QDs, both with and without PhC, as well as with varying B_{ex}. The observed emission rate inhibition in this sample ranges up to more than 10 times which is consistent with the reported values different types of PhCs [136, 143–145]. The large variation of the radiative rate in the data is most likely due to a combination of dot-to-dot variation and also due to the variation of the local density of states depending on the position of the QD on the PhC [145].

In Fig. 5.3, we can see a number of features in E_x^Z associated with the change in τ_R and B_{ex}. Observed under all experimental conditions, the magnitude of E_x^Z decreases with increasing τ_R, reaching a minimum, under both RCP and LCP excitation. As τ_R increases, there is less number of excitation and deexcitation processes per unit time and so less transfer of spin from the electron to the nuclei resulting in lower degree of nuclear spin polarization, therefore smaller E_x^Z.

Under a finite external magnetic field, there is a y-offset due to the Zeeman shift by the permanent magnetic field giving an average of about 7 μeV and 16 μeV for 0.07 T and 0.15 T respectively. In addition, data scattering is observed especially around the 1 – 4 ns region, showing that E_x^Z takes a range of values even for similar τ_R.

Regarding the DOP plotted in Fig. 5.4, in each case, we find an initial decrease in a range τ_R $<\sim$2 ns. This observation reflects the decreasing effective spin polarization due to spin dephasing. Due to the electron spins precession around the "frozen" nuclear field fluctuations, the degree of electron spin polarization as measured from the DOP decreases to 1/3 of its initial value within the dephasing time of the order of 1 ns [31]. Around this timescale, a short radiative lifetime means that spin experiences less dephasing and vice versa.

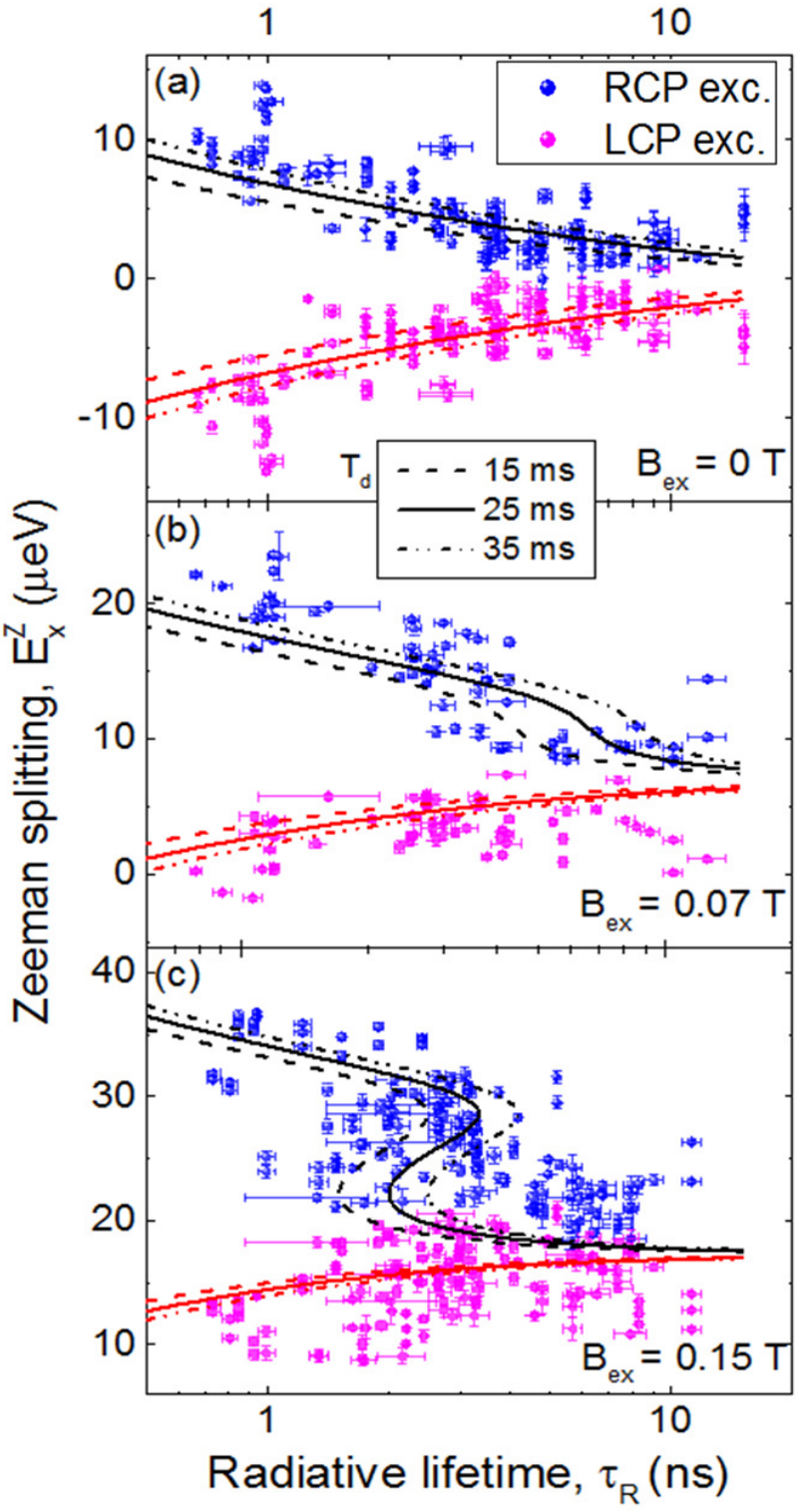

Figure 5.3: Plots of the change of Zeeman splitting and (d-f) degree of polarization with the radiative lifetime on a semilog scale for B_{ex} = 0, 0.07 and 0.15 T. Blue (magenta) spheres and black (red) lines correspond to experimental and simulation results under RCP (LCP) excitation respectively. The solid and broken lines are simulations obtained for different values of T_d as labelled. Other parameter values are fixed: $S_z = 0.14$, $g_e = 0.7$, $\tau_{el} = 320$ ps, $n_e = 0.86$ and N = 3.5× 10^5.

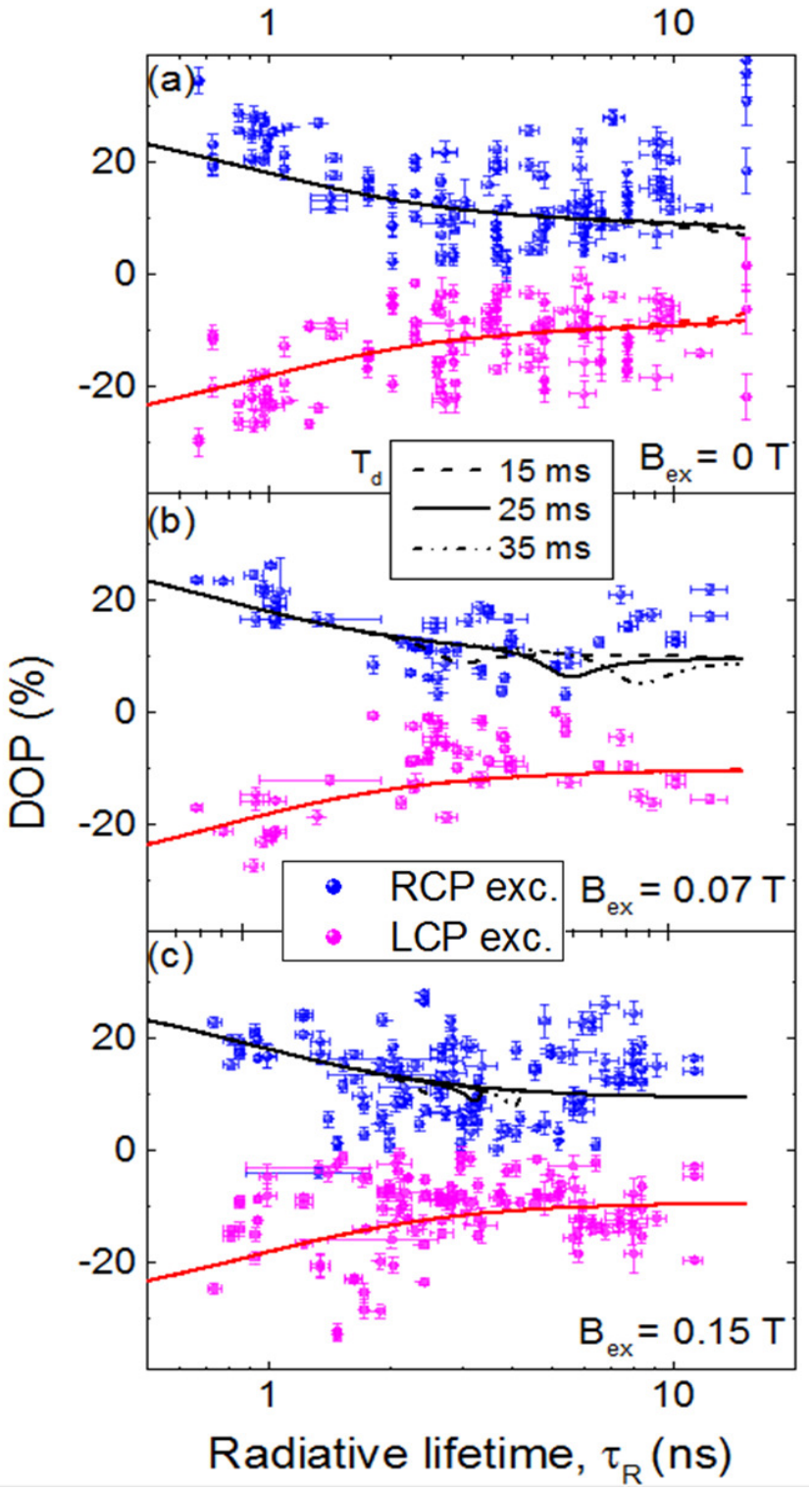

Figure 5.4: Plots of the change of degree of polarization with the radiative lifetime on a semilog scale for $B_{ex} = 0$, 0.07 and 0.15 T. Blue (magenta) spheres and black (red) lines correspond to experimental and simulation results under RCP (LCP) excitation respectively. The solid and broken lines are simulations obtained for different values of T_d as labelled. Other parameter values are fixed: $S_z = 0.14$, $g_e = 0.7$, $\tau_{el} = 320$ ps, $n_e = 0.86$ and N $= 3.5 \times 10^5$.

5.3 Modelling the responses with radiative lifetime

5.3.1 Nuclear spin response

To verify the radiative lifetime dependence of E_x^Z and DOP, we performed simulations using a rate equation model for the coupled electron-nuclear spin system including a decay channel due to coupling to the environment. We apply the rate equation for the dynamic equilibrium between the electron and nuclear spin described in Sec. 3.4.

By expressing $f_{el} = n_e\tau_{el}/\tau_R$ [71], where n_e is the electron density, we could introduce an explicit τ_R dependence into T_{1e} and thus the rate equation. The explicit τ_R dependence will also naturally be incorporated into the steady state solution of $\langle I_z\rangle$ [73]

$$\langle I_z\rangle = \frac{4}{3}\langle S_z\rangle \frac{\overline{I^i(I^i+1)}}{1+\left(\frac{N\hbar}{\bar{A}_i}\right)^2 \frac{\tau_R}{n_e\tau_{el}^2}\frac{1}{T_d}\left[1+\left(\frac{\tau_{el}}{\hbar}\right)^2\left(g_e^*\mu_B B+\bar{A}_i\langle I_z\rangle\right)^2\right]}. \tag{5.1}$$

Again the OS is then given by the relation $\mathrm{OS} = g_e\mu_B B_N = 2\bar{A}_i\langle I_z\rangle$ [59].

For the simulations, values of QD parameters are chosen within constrained ranges in accordance to values reported in the literature [59, 73, 127]: $\bar{A}_i$=50 μeV, $\overline{I^i(I^i+1)}$=13.2, $S_z = 0.14$, $g_e = -0.7$, $\tau_{el} = 320$ ps, $n_e = 0.86$ and N = 3.5×10^4. There is a certain inhomogeneity in the parameters as measurements were performed on many single QDs. Following from this, since T_d is expected to be the parameter that varies most significantly from QD to QD [119], we also simulated curves with different T_d.

The simulation results are also plotted in Fig. 5.3 and 5.4, which reproduces the main feature of increasing E_x^Z and DOP with decreasing τ_R, validating the τ_R dependence in this model. Simulations for different T_d allow us to partially account for the spread in the experimental data, especially for E_x^Z. Under applied magnetic fields, the simulated curves exhibits winding in their curves. This arises from the existence of multiple configurations of the nuclear spin ensemble, analogous to bistability behaviour with respect to τ_R [70, 71, 73].

5.3.2 Nuclear spin bistability with respect to radiative lifetime

A key requirement to observe bistability in the nuclear spin polarization is the negative feedback in the electron-nuclear spin system. In the case of RCP excitation, with the external field and nuclear field parallel this negative feedback is present: an increase in τ_R decreases B_n, which in turn reduces the energy mismatch between the electron and the nuclear spin, therefore facilitating mutual spin flip-flops. Within the bistability regime, there exist two observable nuclear spin polarization configurations for a given τ_R, accompanied by abrupt increase or decrease at the "edge" of the regime. The feature of E_x^Z at 0.07 T could be the onset of bistability behaviour while the two "columns" of scattered data points along 2 and 3 ns at 0.15 T could correspond to the abrupt increase and decrease of nuclear spin polarization, marking the edges of the bistability regime. Figure 5.5 gives an intuitive understanding of how bistability arises by looking at the mathematical form of the steady state solution of $\langle I_z \rangle$ (eqn. 5.1).

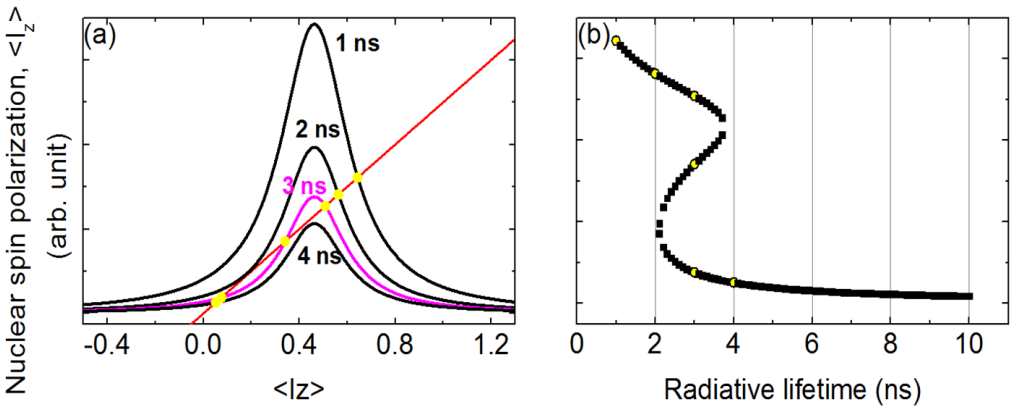

Figure 5.5: To illustrate the bistability of the nuclear field with respect to the radiative lifetime, the above plots are produced using a different set of parameters $S_z = 0.2$, $g_e = -2$, $\tau_{el} = 90$ ps, $n_e = 0.1$ and N = 2.0×10^4, T_d =50 ms and B_{ex} =0.2 T. (a) The lorentzian curves represent the right hand side of the steady state solution for different values of τ_R as labelled while the red line represents the left hand side of the solution. The intersection between the curves and the straight line gives solutions of nuclear spin configuration. For the case of $\tau_R = 3$ ns, there are 3 intersections, as opposed to only one intersection for the other τ_R. (b) Plot of the $\langle I_z \rangle$ values of the intersection points over a range of τ_R showing an "inverted-S" behaviour characteristic of bistability. The points highlighted as yellow circles correspond to the intersection points in (a). For the range of τ_R where 3 solutions exist, the high and low values of $\langle I_z \rangle$ are stable solutions and are thus observable.

5.3.3 Degree of polarization response

The procedure to calculate DOP follows that in reference [74], *i.e.* where we consider the frozen field model, in which the electron spin precesses about the random nuclear field, δB_n (typically of the order of tens of milli-Tesla) with a characteristic dephasing time. This dephasing time can be thought of as the electron ensemble decoherence time as experiments constitute an average over many measurements. In each measurement, the electron is subjected to different random nuclear magnetic field. The typical dephasing time is of the order of $T_\Delta = 0.5{-}1$ ns. As such, the time-integrated DOP of X^+ is given by:

$$DOP = 2/\tau_R \int \langle S_z(t) \rangle \, \exp(t/\tau_R) dt, \tag{5.2}$$

where $\langle S_z(t) \rangle$ is the electron spin evolution averaged over the distribution of random nuclear fields expressed by the following equation ([31]:

$$\langle S_z(t) \rangle = \frac{\langle S_z \rangle}{3} \left\{ 1 + 2 \left[1 - 2 \left(\frac{t}{T_\Delta} \right)^2 \right] \exp \left[- \left(\frac{t}{T_\Delta} \right)^2 \right] \right\}. \tag{5.3}$$

The flip-flop rate for a photogenerated X^+ electron interacting with N nuclei, including the first order spin relaxation mechanism can be deduced from Eq. (3.11) and (3.12) as

$$\frac{1}{T_{ff}} = \frac{4}{3} \frac{\overline{I^i(I^i+1)} N}{f_{el}} \frac{1}{T_{1e}} \left\{ 1 / \left[1 + \left(\frac{E_x^Z}{g_e \mu_B \delta B_n} \right)^2 \right] \right\}. \tag{5.4}$$

T_{ff} can be thought of at the average time it takes for one single electron-nuclear spin flip. The term $\langle S_z \rangle$ in Eq. (5.2) is modified to include the spin relaxation term as: $\langle S_z \rangle \rightarrow \langle S_z \rangle / (1 + \tau_R / T_{ff})$.

Dips in DOP curves correspond to where the electron-nuclear spin flip-flop time is close to τ_R (Fig. 5.4). Here, each excitation is likely to be followed by a spin flip event. A flipped spin before radiative recombination gives emission of the opposite polarization and when averaged out over many cycles, this results in lower DOP. These simulated features of the multiple nuclear spin configurations and dips in the DOP could partially account for the data scattering observed in the experiments. However, the main contribution is most likely the inhomogeneity in QD characteristics.

5.3.4 Towards higher degree of nuclear spin polarization: the case for short radiative lifetimes

Given the influence of τ_R on DNP, it is worth investigating the maximum achievable nuclear spin polarization simply via τ_R modification. Since, the mechanism of DNP involves the electron spin injection rate, electron removal rate and the spin transfer rate, to investigate the optimum τ_R for DNP, we performed simulations at short τ_R. To take into account of the situation where the short τ_R becomes the limiting factor of the electron-nuclear spin correlation time, we explicitly express τ_{el} in a form of $1/\tau_{el} = 1/\tau_{el}^0 + 1/\tau_R$, where τ_{el}^0 consist of contribution from all other processes besides τ_R (e.g. spin relaxation, charge fluctuation) [146].

Figure 5.6 shows a simulation with the same parameters as in Fig. 5.3(c). As τ_R is reduced from 1 ns, the increasing spin injection rate helps to achieve higher magnitude of Zeeman splitting up to a maximum. The optimum range of τ_R for most efficient DNP occurs where $\tau_R \sim \tau_{el}^0$. In this range, the τ_R allows for minimally sufficient interaction time between the electron and nuclear spins while maintaining a well-defined electron spin and large enough electron spin broadening. Reducing τ_R even further results in decreasing OS. At this stage, there is too little time for the electron and nuclear spins to interact. Even with a lot of spin injection events, the low probability of mutual spin flip gives inefficient DNP. In constrast, with a constant τ_{el}, the magnitude of OS increases monotonically with decreasing τ_R which is unphysical. Additional feature of multiple nuclear spin configurations can seen at longer τ_R around 2 ns.

As for DOP, reducing τ_R simply increases it up to saturation. At short τ_R, the electron completely preserve its spin information which is then transffered into the emission polarization. In the multi-nuclear spin configuration the ratio τ_R/T_{ff} approaches 1 signifying almost one electron-nuclear spin flip per excitation.

As can be seen in Fig. 5.7, higher external magnetic field causes the maximum OS to shift to lower τ_R while also reducing its magnitude. Based on these simulations, depending on the QD and experimental parameter values, the regime of DNP that is routinely access in the reports for bare QDs with $\tau_R = 0.6 - 1$ ns is not always optimum. This highlights the importance of engineering the optimum τ_R to achieve high DNP. One way to attain optimum τ_R is by using cavity effect such as the Purcell enhancement [136, 143, 144]. Given the reported Purcell enhancement factor of about a few tens [147], the enhanced emission rate should allow us to access the maximum achievable DNP.

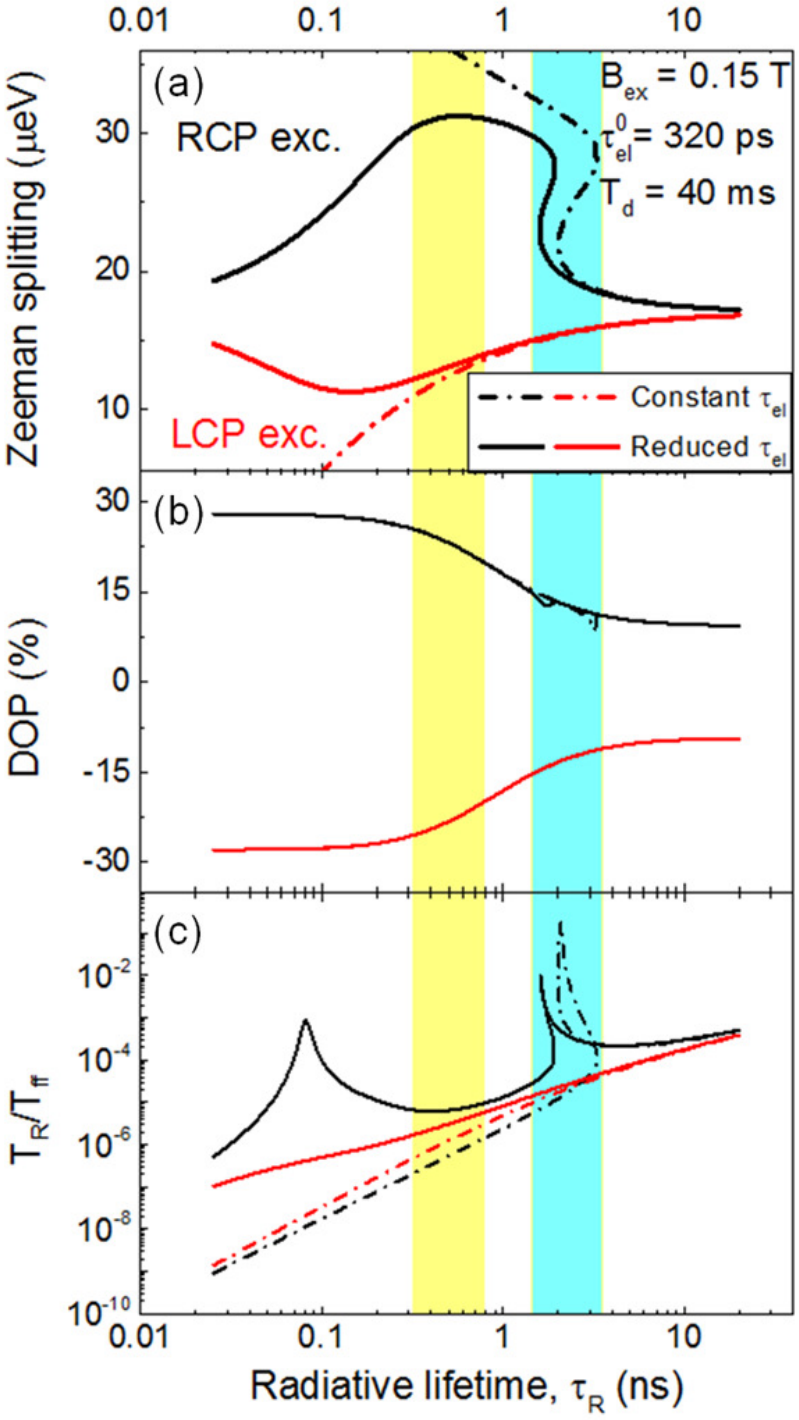

Figure 5.6: Simulation results of (a)Zeeman splitting, (b)DOP and (c)ratio τ_R/T_{ff} vs τ_R under RCP (black) and LCP (red) excitation, carried out with with $B_{ex} = 0.15$ T, $T_d = 40$ ms, $S_z = 0.14$, $g_e = 0.7$, $\tau_{el} = 320$ ps, $n_e = 0.86$, N $= 3.5\times10^4$, $T_\Delta = 1.9$ ns and $\delta B_n = 7$ mT. Solid (dashed) lines correspond to using explicit (constant) τ_{el} in simulations. The region shaded in yellow shows optimum range of τ_R for maximum degree of nuclear spin polarization. The maximum OS is achieved at different τ_R under RCP and LCP excitation due to the breaking of symmetry by B_{ex}. The region in light blue shade shows the occurrence of bistability.

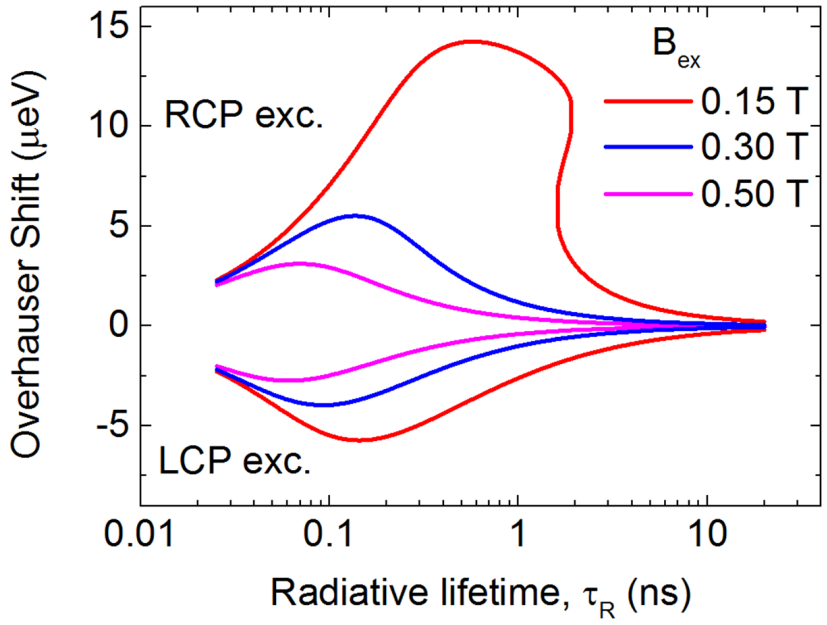

Figure 5.7: Plot showing the response of the OS against τ_R under different external magnetic field suggesting how the optimum DNP requires lower τ_R at higher fields. Other simulation parameters are as follows: T_d = 40 ms, S_z = 0.14, g_e = 0.7, τ_{el} = 320 ps, n_e = 0.86, N = 3.5×10^4.

5.4 Summary and outlook

In summary, by measuring the change in E_x^Z and DOP with τ_R, we showed that engineering of photonic environment using PhC can be used to control the dynamics of nuclear spin polarization. Shorter τ_R is favourable to obtain high nuclear spin polarization. A viable next step is to introduce nanocavities to achieve high Purcell factor leading to higher degree of nuclear spin polarization without the use of complex excitation scheme.

Our work suggests the possibility of realizing a high degree of nuclear polarization through the DNP via exciton lifetime modulation and thus has immediate implications on the study of the integration of QD in PhC for spin-photon interfaces [148–151] and scalable quantum computing [95, 152, 153].

In addition to accessing short radiative lifetimes for higher nuclear spin polarization, the use of cavity allows for the observation of the change in DNP with radiative lifetime with a single QD which could eliminate the scattering that arises from multi-QD measurements. However, the use cavity imposes further experimental constraints such as spatial and spectral matching. Technologies of site-controlled QD [154] and QD position detection [155] will pave the way to circumventing the problems with spatial matching between QD and local electric field in the photonic crystal. We could also relax the conditions for spectral matching by using a cavity of a lower Q-factor and thus broader

resonance. For a standard PhC nanocavity with a mode volume of $\sim 0.5(\lambda/n)^3$, where λ is the resonant frequency and n is the refractive index, a low Q factor of $\sim$100 is enough to obtain a Purcell factor of $\sim$10, which is large enough to access the maximum possible nuclear spin polarization given the current experimental conditions and parameter values. In this case, the stringent conditions for the spectral matching are mitigated as the cavity possesses a large bandwidth for the Purcell effect. The enhancement of emission rate to modify DNP can also be achieved using plasmonic effects, with the added benefit of a small structure footprint as compared to photonic cavities [156].

Chapter 6

Conclusion and outlook

Self-assembled quantum dots possess attractive properties for various applications, in particular spin-based technologies such as spintronics and quantum information. The confined carrier spins are the main resource in these technologies, however, the fluctuating nuclear spin ensemble in the QD causes carrier spin dephasing. This issue can be addressed by manipulating the nuclear spins. In this thesis, we have investigated the optical orientation of the electron spin confined in a QD for the purpose of manipulating the nuclear spin dynamics. We looked at 3 different approaches: 1) dealing with the energy states of QD by p-shell carrier excitation 2) modifiying the mechanism of DNP and 3) using OAM of light as a new degree of freedom of excitation.

We demonstrated that even without any applied external magnetic field, the electrons in the p-shell of the QD can polarize the nuclear spins. We probed the nuclear spin buildup time using circular polarization modulation excitation, enabling us to extract temporal dynamics from time-averaged measurements. In addition to mutual spin flips with the nuclei, the p-shell electrons reduce nuclear spin diffusion out of the QD due to the inhomogeneity in its spatial wavefunction. These effects of the p-shell electrons are reflected in the abrupt increase in the nuclear spin buildup time, together with the increase of OS with p-shell emission intensity. The limited spatial extent of the s-shell electrons could be aided by that of the p-shell electrons and the combined effect is such that the electrons from both shells together interact and thus polarize an overall larger number of nuclear spins.

Besides the spatial wavefunction, the QD emission radiative rate is another limiting factor of the degree of nuclear spin polarization. By controlling the QD emission radiative rate using the photonic bandgap effect of a photonic crystal, we manipulated the achievable degree of nuclear spin polarization. A higher radiative rate gives more spin transfer from the electron to the nuclei which results in larger nuclear spin polarization and vice versa. Furthermore, we observed the nonlinear behaviour of the nuclear spins with radiative rate

such as the presence of multiple spin configurations even at a small applied external magnetic field of a few tens of milliTesla.

Photonic crystal nanocavity enables us to use twisted light to manipulate the nuclear spins. By embedding the QD in a suitably designed PhC nanocavity, we could couple twisted light excitation to the cavity modes. By having a QD coupled to the cavity, the orbital angular momentum in the twisted light can be transferred into the QD as carrier spins in accordance to conservation of angular momentum. We have outlined such an OAM-to-SAM converter scheme – the physical mechanisms and experimental requirements – with PhC nanocavity, twisted light and QD as our main components. We proposed to use this scheme for the optical spin pumping to polarize the nuclear spins in the QD.

As mentioned in chapter 1, the formation of nuclear spin dark states which is insensitive to the hyperfine contact interaction has been proposed as a possible factor limiting the complete polarization of nuclear spins [54, 87]. Along with this idea, it was also proposed that the solution to the nuclear spin dark states is by modifying the spatial wavefunction of the confined electron using external electric field and/or having an inhomogeneous Knight field [86]. We could instead excite p-shell electrons in place of using external electric field. The p-shell electrons have a different spatial wavefunction compared to that of s-shell electrons, which could possibly give the same effect as modifying the electron wavefunction with external electric fields. Furthermore, the short p-shell electron lifetime would broaden its spin state which is known to improve the efficiency of electron-nuclear spin flip. For this purpose, it is worth to further investigate the polarization or the spin configuration of the p-shell states, in order for deterministic optical orientation of the p-shell electrons. As such, our results on DNP by p-shell electrons could give insights to allow us to verify the concept of nuclear spin dark states and possibly a means to couple to these states.

The demonstration of manipulation of nuclear spin polarization degree with the photonic bandgap effect paves the way for further work of active control of the nuclear spin dynamics. By enhancing the radiative rate using the Purcell effect exhibited by coupling between QD with cavity or plasmonic effects, we could achieve higher degree of nuclear spin polarization. This active control could even be utilized as a switch [157] to allow us to tune the radiative rate to access the regime of highly polarized nuclear spin. By exploiting the high radiative rate, A QD embedded in a PhC nanocavity could first have its nuclear spin polarized to a high degree before an electron spin state is initialized. The reduced nuclear spin fluctuation and the generated strong nuclear field are

both advantageous for long electron spin lifetime. They could also reduce the need for large applied external magnetic field so often used to alleviate electron spin dephasing.

Quick ejection of the electron to leave an "empty" or "dark" QD has been found to allow the nuclear spin to remain coherent for long periods of time of up to 1s [83, 158]. While complete nuclear spin polarization is an important requirement, the coherence of the nuclear spin is indispensable to realize a functional quantum memory device [80]. In light of this, Purcell enhanced high radiative rate and consequently short radiative lifetime could allow for a quick removal of the electron after "saving" its state as nuclear spin states, ensuring that the nuclear spin states can remain coherent long relative to gate operation times. Here the quick electron removal is a passive process in contrast with active electrical switching with a microseconds long pulse in charge-tunable QDs [63]. Such possibility afforded by the control of the radiative rate could mean a memory device with operation speeds in excess of 1 GHz, limited by the radiative rate.

It has been proposed theoretically that twisted light could induce precise "diagonal" transitions in a QD where interband transitions are also accompanied by a change in the shell, for example an electron can be excited from the heavy hole [159] or light hole [160] valence s-shell to the conduction p-shell. Therefore, twisted light holds the promise for selective excitation of p-shell carriers. In addition, such transitions can also be a key component in a nuclear spin-based quantum memory and spin-photon interface, where the entangled twisted light first transfer its quantum state to a confined electron spin which then passes it to the nuclei for storage and retrieval. However, since the transition is relatively weak, it may be necessary to make use of nanostructures such as a PhC nanocavity or plasmonic grating [161].

The coupled electron-nuclear spin system in a QD contains rich physics, even more so when the QD is embedded in a photonic nanostructure. As much as it is an imperative to understand the system in order to utilize it for practical application, we should also appreciate the wonder of exploration and discovery, true to the spirit of science.

Bibliography

1. Commins, E. D. "Electron Spin and Its History". *Annual Review of Nuclear and Particle Science* **62,** 133–157 (2012) (pg. 1).
2. Uhlenbeck, G. E. & Goudsmit, S. "Spinning Electrons and the Structure of Spectra". *Nature* **117,** 264–265 (1925) (pg. 1).
3. Knight, W. D. "Nuclear Magnetic Resonance Shift in Metals". *Physical Review* **76,** 1259–1260 (1949) (pg. 1).
4. Overhauser, A. W. "Polarization of Nuclei in Metals". *Physical Review* **92,** 411–415 (1953) (pg. 1).
5. Lampel, G. "Nuclear dynamic polarization by optical electronic saturation and optical pumping in semiconductors". *Physical Review Letters* **20,** 491–493 (1968) (pg. 1).
6. Telford, M. "QD lasers go to market". *III-Vs Review* **17,** 28–31 (2004) (pg. 2).
7. Chen, H., He, J. & Wu, S.-T. "Recent Advances on Quantum-Dot-Enhanced Liquid Crystal Displays". *IEEE Journal of Selected Topics in Quantum Electronics* **23,** 1–1 (2017) (pg. 2).
8. Loss, D. & DiVincenzo, D. P. "Quantum computation with quantum dots". *Physical Review A* **57,** 120–126 (1998) (pg. 2).
9. Santori, C., Pelton, M., Solomon, G., Dale, Y. & Yamamoto, Y. "Triggered Single Photons from a Quantum Dot". *Physical Review Letters* **86,** 1502–1505 (2001) (pg. 2).
10. Chen, G. "Optically Induced Entanglement of Excitons in a Single Quantum Dot". *Science* **289,** 1906–1909 (2000) (pg. 2).
11. Jennewein, T, Simon, C, Weihs, G, Weinfurter, H & Zeilinger, a. "Quantum cryptography with entangled photons". *Physical review letters* **84,** 4729–32 (2000) (pg. 2).
12. Gao, W. *et al.* "Quantum teleportation from a propagating photon to a solid-state spin qubit". *Nature Communications* **4** (2013) (pg. 2).
13. Atature, M. *et al.* "Quantum-dot spin-state preparation with near-unity fidelity." *Science* **312,** 551–3 (2006) (pg. 2).
14. DiVincenzo, D. P. "The Physical Implementation of Quantum Computation". *Fortschritte der Physik* **48,** 771–783 (2000) (pg. 2).
15. Kloeffel, C. & Loss, D. "Prospects for Spin-Based Quantum Computing in Quantum Dots". *Annual Review of Condensed Matter Physics* **4,** 51–81 (2013) (pg. 2).

16. Petta, J. R. *et al.* "Coherent Manipulation of Coupled Electron Spins in Semiconductor Quantum Dots". *Science* **309,** 2180–2184 (2005) (pg. 2, 3).

17. Kroutvar, M. *et al.* "Optically programmable electron spin memory using semiconductor quantum dots". *Nature* **432,** 81–84 (2004) (pg. 2).

18. Elzerman, J. M. *et al.* "Single-shot read-out of an individual electron spin in a quantum dot". *Nature* **430,** 431–435 (2004) (pg. 2).

19. Greilich, A *et al.* "Mode Locking of Electron Spin Coherence in Singly Charged Quantum Dots." *Science* **313,** 341–345 (2006) (pg. 2).

20. Meier, F & Zakharchenya, B. P. *Modern Problems in Condensed Matter Sciences Vol. 8 Optical Orientation* (North-Holland, Amsterdam, 1984) (pg. 2–4, 11, 15, 19, 22).

21. Burkard, G., Loss, D. & DiVincenzo, D. P. "Coupled quantum dots as quantum gates". *Physical Review B* **59,** 2070–2078 (1999) (pg. 2).

22. Khaetskii, A. V. & Nazarov, Y. V. "Spin relaxation in semiconductor quantum dots". *Physical Review B* **61,** 12639–12642 (2000) (pg. 2).

23. Khaetskii, A. V. & Nazarov, Y. V. "Spin-flip transitions between Zeeman sublevels in semiconductor quantum dots". *Physical Review B* **64,** 7 (2001) (pg. 2).

24. Paillard, M. *et al.* "Spin relaxation quenching in semiconductor quantum dots". *Physical Review Letters* **86,** 1634–1637 (2001) (pg. 2).

25. Amasha, S. *et al.* "Electrical control of spin relaxation in a quantum dot". *Physical Review Letters* **100,** 1–4 (2008) (pg. 2).

26. Le Gall, C., Brunetti, A., Boukari, H. & Besombes, L. "Electron-nuclei spin dynamics in II-VI semiconductor quantum dots". *Physical Review B* **85,** 195312 (2012) (pg. 2, 23).

27. Whitaker, K. M. *et al.* "Hyperfine Coupling in Colloidal n-Type ZnO Quantum Dots : Effects on Electron Spin Relaxation". *J. Chem. Phys.* **114,** 14467–14472 (2010) (pg. 2).

28. Schliemann, J., Khaetskii, A. V. & Loss, D. "Electron spin dynamics in quantum dots and related nanostructures due to hyperfine interaction with nuclei". *Journal of Physics: Condensed Matter* **15,** R1809–R1833 (2003) (pg. 2).

29. Dyakanov, M. I. & Perel, V. I. "Theory of Optical Spin Orientation of Electrons and Nuclei in Semiconductors". *Zh. Eksp. Teor. Fiz.* **65,** 362–375 (1973) (pg. 3, 21, 22).

30. Johnson, A. C. *et al.* "Triplet-singlet spin relaxation via nuclei in a double quantum dot." *Nature* **435,** 925–8 (2005) (pg. 3).

31. Merkulov, I. A., Efros, A. L. & Rosen, M. "Electron spin relaxation by nuclei in semiconductor quantum dots". *Physical Review B* **65,** 205309 (2002) (pg. 3, 18, 41, 46).

32. Braun, P. *et al.* "Direct Observation of the Electron Spin Relaxation Induced by Nuclei in Quantum Dots". *Physical Review Letters* **94,** 116601 (2005) (pg. 3, 26).

33. Dutt, M. V. G. *et al.* "Stimulated and spontaneous optical generation of electron spin coherence in charged GaAs quantum dots". *Physical Review Letters* **94,** 1–4 (2005) (pg. 3).

34. Lombez, L *et al.* "Electron spin quantum beats in positively charged quantum dots: nuclear field effects". *Physical Review B* **75,** 10 (2007) (pg. 3).

35. Bechtold, A. *et al.* "Three-stage decoherence dynamics of an electron spin qubit in an optically active quantum dot". *Nature Physics* **11,** 1005–1008 (2015) (pg. 3).

36. Koppens, F. H. L. "Control and Detection of Singlet-Triplet Mixing in a Random Nuclear Field". *Science* **309,** 1346–1350 (2005) (pg. 3).

37. Shenvi, N., De Sousa, R. & Whaley, K. B. "Universal scaling of hyperfine-induced electron spin echo decay". *Physical Review B - Condensed Matter and Materials Physics* **71,** 1–8 (2005) (pg. 3).

38. Koppens, F. H. L., Nowack, K. C. & Vandersypen, L. M. K. "Spin echo of a single electron spin in a quantum dot". *Physical Review Letters* **100,** 1–4 (2008) (pg. 3).

39. Press, D. *et al.* "Ultrafast optical spin echo in a single quantum dot". *Nature Photonics* **4,** 367–370 (2010) (pg. 3).

40. Fischer, J., Coish, W. A., Bulaev, D. V. & Loss, D. "Spin decoherence of a heavy hole coupled to nuclear spins in a quantum dot". *Physical Review B - Condensed Matter and Materials Physics* **78,** 1–9 (2008) (pg. 3).

41. Testelin, C., Bernardot, F., Eble, B. & Chamarro, M. "Hole–spin dephasing time associated with hyperfine interaction in quantum dots". *Physical Review B* **79,** 195440 (2009) (pg. 3).

42. Eble, B. *et al.* "Hole–Nuclear Spin Interaction in Quantum Dots". *Physical Review Letters* **102,** 146601 (2009) (pg. 3).

43. Brunner, D. *et al.* "A Coherent Single-Hole Spin in a Semiconductor". *Science* **325,** 70–73 (2009) (pg. 3).

44. Heiss, D. *et al.* "Observation of extremely slow hole spin relaxation in self-assembled quantum dots". *Physical Review B* **76,** 241306 (2007) (pg. 3).

45. Godden, T. M., Boyle, S. J., Ramsay, A. J., Fox, A. M. & Skolnick, M. S. "Fast high fidelity hole spin initialization in a single InGaAs quantum dot". *Applied Physics Letters* **97,** 061113 (2010) (pg. 3).

46. De Greve, K. *et al.* "Ultrafast coherent control and suppressed nuclear feedback of a single quantum dot hole qubit". *Nature Physics* **7,** 872–878 (2011) (pg. 3).

47. Gerardot, B. D. *et al.* "Optical pumping of a single hole spin in a quantum dot." *Nature* **451,** 441–4 (2008) (pg. 3).

48. Coish, W. & Loss, D. "Hyperfine interaction in a quantum dot: Non-Markovian electron spin dynamics". *Physical Review B* **70,** 195340 (2004) (pg. 3).

49. Klauser, D., Coish, W. A. & Loss, D. "Nuclear spin state narrowing via gate-controlled Rabi oscillations in a double quantum dot". *Physical Review B - Condensed Matter and Materials Physics* **73,** 1–12 (2006) (pg. 3).

50. Stepanenko, D., Burkard, G., Giedke, G. & Imamoglu, A. "Enhancement of electron spin coherence by optical preparation of nuclear spins". *Physical Review Letters* **96,** 136401 (2006) (pg. 3).

51. Greilich, A. *et al.* "Nuclei-Induced Frequency Focusing of Electron Spin Coherence". *Science* **317,** 1896–1899 (2007) (pg. 3).

52. Xu, X. *et al.* "Optically controlled locking of the nuclear field via coherent dark-state spectroscopy." *Nature* **459,** 1105–9 (2009) (pg. 3, 5, 6).

53. Khaetskii, A. V., Loss, D. & Glazman, L. "Electron spin evolution induced by interaction with nuclei in a quantum dot". *Physical Review B* **67,** 195329 (2003) (pg. 3, 5).

54. Imamoglu, A., Knill, E., Tian, L. & Zoller, P. "Optical Pumping of Quantum-Dot Nuclear Spins". *Physical Review Letters* **91,** 017402 (2003) (pg. 3, 6, 52).

55. Brown, S. W., Kennedy, T. A., Gammon, D. & Snow, E. S. "Spectrally resolved Overhauser shifts in single GaAs/AlxGa1-xAs quantum dots". *Physical Review B* **54,** R17339–R17342 (1996) (pg. 3).

56. Gammon, D. "Nuclear Spectroscopy in Single Quantum Dots: Nanoscopic Raman Scattering and Nuclear Magnetic Resonance". *Science* **277,** 85–88 (1997) (pg. 3).

57. Gammon, D. *et al.* "Electron and Nuclear Spin Interactions in the Optical Spectra of Single GaAs Quantum Dots". *Physical Review Letters* **86,** 5176–5179 (2001) (pg. 3).

58. Bracker, A. S. *et al.* "Optical Pumping of the Electronic and Nuclear Spin of Single Charge-Tunable Quantum Dots". *Physical Review Letters* **94,** 047402 (2005) (pg. 3, 21).

59. Eble, B. *et al.* "Dynamic nuclear polarization of a single charge-tunable InAs/GaAs quantum dot". *Physical Review B* **74,** 081306 (2006) (pg. 3, 5, 23, 34, 44).

60. Cherbunin, R. V. *et al.* "Dynamics of the nuclear spin polarization by optically oriented electrons in a (In,Ga)As/GaAs quantum dot ensemble". *Physical Review B* **80,** 035326 (2009) (pg. 3, 20, 23, 30, 37).

61. Ono, K. & Tarucha, S. "Nuclear-Spin-Induced Oscillatory Current in Spin-Blockaded Quantum Dots". *Physical Review Letters* **92,** 256803 (2004) (pg. 3).

62. Baugh, J., Kitamura, Y., Ono, K. & Tarucha, S. "Large nuclear overhauser fields detected in vertically coupled double quantum dots". *Physical Review Letters* **99,** 2–5 (2007) (pg. 3).

63. Maletinsky, P., Badolato, A. & Imamoglu, A. "Dynamics of Quantum Dot Nuclear Spin Polarization Controlled by a Single Electron". *Physical Review Letters* **99,** 056804 (2007) (pg. 3, 22, 30, 53).

64. Tartakovskii, A. I. *et al.* "Nuclear Spin Switch in Semiconductor Quantum Dots". *Physical Review Letters* **98,** 026806 (2007) (pg. 3–5).

65. Auer, T. *et al.* "Measurement of the Knight field and local nuclear dipole-dipole field in an InGaAs/GaAs quantum dot ensemble". *Physical Review B* **80,** 205303 (2009) (pg. 3).

66. Huang, C.-W. & Hu, X. "Theoretical study of nuclear spin polarization and depolarization in self-assembled quantum dots". *Physical Review B* **81,** 205304 (2010) (pg. 4, 19).

67. Lai, C. W., Maletinsky, P., Badolato, A. & Imamoglu, A. "Knight-Field-Enabled Nuclear Spin Polarization in Single Quantum Dots". *Physical Review Letters* **96,** 167403 (2006) (pg. 4, 5).

68. Dzhioev, R. I. & Korenev, V. L. "Stabilization of the Electron-Nuclear Spin Orientation in Quantum Dots by the Nuclear Quadrupole Interaction". *Physical Review Letters* **99,** 037401 (2007) (pg. 4, 19).

69. Chekhovich, E. A., Hopkinson, M, Skolnick, M. & Tartakovskii, A. I. "Suppression of nuclear spin bath fluctuations in self-assembled quantum dots induced by inhomogeneous strain". *Nature Communications* **6,** 6348 (2015) (pg. 4, 19).

70. Braun, P. *et al.* "Bistability of the nuclear polarization created through optical pumping in In1-xGaxAs quantum dots". *Physical Review B* **74,** 245306 (2006) (pg. 4, 44).

71. Kaji, R., Adachi, S., Sasakura, H. & Muto, S. "Hysteretic response of the electron nuclear spin system in single In0.75Al0.25As quantum dots: Dependences on excitation power and polarization". *Physical Review B* **77,** 115345 (2008) (pg. 4, 44).

72. Belhadj, T. *et al.* "Optically monitored nuclear spin dynamics in individual GaAs quantum dots grown by droplet epitaxy". *Physical Review B* **78,** 205325 (2008) (pg. 4, 22).

73. Maletinsky, P., Lai, C. W., Badolato, A. & Imamoglu, A. "Nonlinear dynamics of quantum dot nuclear spins". *Physical Review B* **75,** 035409 (2007) (pg. 4, 5, 44).

74. Krebs, O. *et al.* "Hyperfine interaction in InAs/GaAs self-assembled quantum dots: dynamical nuclear polarization versus spin relaxation". *Comptes Rendus Physique* **9,** 874–884 (2008) (pg. 4, 46).

75. Latta, C. *et al.* "Confluence of resonant laser excitation and bidirectional quantum-dot nuclear-spin polarization". *Nature Physics* **5,** 758–763 (2009) (pg. 5, 6).

76. Hogele, A. *et al.* "Dynamic Nuclear Spin Polarization in the Resonant Laser Excitation of an InGaAs Quantum Dot supp". *Physical Review Letters* **108,** 197403 (2012) (pg. 5).

77. Ebbens, A. *et al.* "Optical orientation and control of spin memory in individual InGaAs quantum dots". *Physical Review B* **72,** 073307 (2005) (pg. 5).

78. Oulton, R. *et al.* "Polarized quantum dot emission from photonic crystal nanocavities studied under moderesonant enhanced excitation." *Optics express* **15,** 17221–17230 (2007) (pg. 5).

79. Taylor, J. M., Marcus, C. M. & Lukin, M. D. "Long-Lived Memory for Mesoscopic Quantum Bits". *Physical Review Letters* **90,** 206803 (2003) (pg. 5).

80. Schwager, H., Cirac, J. I. & Giedke, G. "Quantum interface between light and nuclear spins in quantum dots". *Physical Review B* **81,** 045309 (2010) (pg. 5, 53).

81. Ding, W., Shi, A., You, J. Q. & Zhang, W. "High-fidelity quantum memory utilizing inhomogeneous nuclear polarization in a quantum dot". *Physical Review B* **90,** 235421 (2014) (pg. 5).

82. Malein, R. N. E. *et al.* "Screening Nuclear Field Fluctuations in Quantum Dots for Indistinguishable Photon Generation". *Physical Review Letters* **116,** 257401 (2016) (pg. 5).

83. Wust, G *et al.* "Role of the electron spin in determining the coherence of the nuclear spins in a quantum dot". *Nature Nanotechnology* **11,** 1–6 (2016) (pg. 5, 53).

84. Urbaszek, B. *et al.* "Efficient dynamical nuclear polarization in quantum dots: Temperature dependence". *Physical Review B* **76,** 201301 (2007) (pg. 5, 34).

85. Chekhovich, E. A. *et al.* "Pumping of Nuclear Spins by Optical Excitation of Spin-Forbidden Transitions in a Quantum Dot". *Physical Review Letters* **104,** 066804 (2010) (pg. 6).

86. Christ, H., Cirac, J. I. & Giedke, G. "Quantum description of nuclear spin cooling in a quantum dot". *Physical Review B - Condensed Matter and Materials Physics* **75,** 1–8 (2007) (pg. 6, 52).

87. Hildmann, J., Kavousanaki, E., Burkard, G. & Ribeiro, H. "Quantum limit for nuclear spin polarization in semiconductor quantum dots". *Physical Review B* **89,** 205302 (2014) (pg. 6, 52).

88. Chekhovich, E. A. *et al.* "Measurement of the spin temperature of optically cooled nuclei and GaAs hyperfine constants in GaAs/AlGaAs quantum dots". *Nature Materials* **16** (2017) (pg. 6, 20).

89. Éthier-Majcher, G. *et al.* "Improving a Solid-State Qubit through an Engineered Mesoscopic Environment". *Physical Review Letters* **119,** 130503 (2017) (pg. 6).

90. Rubinsztein-Dunlop, H. *et al.* "Roadmap on structured light". *Journal of Optics* **19,** 013001 (2017) (pg. 7).

91. Cygorek, M., Tamborenea, P. I. & Axt, V. M. "Insensitivity of spin dynamics to the orbital angular momentum transferred from twisted light to extended semiconductors". *Physical Review B - Condensed Matter and Materials Physics* **92,** 1–5 (2015) (pg. 7).

92. Babiker, M, Bennett, C. R., Andrews, D. L. & Dávila Romero, L. C. "Orbital Angular Momentum Exchange in the Interaction of Twisted Light with Molecules". *Physical Review Letters* **89,** 143601 (2002) (pg. 7).

93. Quinteiro, G. F., Lucero, A. O. & Tamborenea, P. I. "Electronic transitions in quantum dots and rings induced by inhomogeneous off-centered light beams". *Journal of Physics: Condensed Matter* **22,** 505802 (2010) (pg. 7).

94. Liu, J. *et al.* "Direct observation of nanofabrication influence on the optical properties of single self-assembled InAs/GaAs quantum dots". *arXiv,* 1–11 (2017) (pg. 7).

95. Carter, S. G. *et al.* "Quantum control of a spin qubit coupled to a photonic crystal cavity". *Nature Photonics* **7,** 329–334 (2013) (pg. 7, 49).

96. Goldstein, L., Glas, F., Marzin, J. Y., Charasse, M. N. & Le Roux, G. "Growth by molecular beam epitaxy and characterization of InAs/GaAs strained-layer superlattices". *Applied Physics Letters* **47,** 1099 (1985) (pg. 10).

97. Heyn, C. "Critical coverage for strain-induced formation of InAs quantum dots". *Physical Review B* **64,** 165306 (2001) (pg. 10).

98. Madhukar, A., Xie, Q., Chen, P. & Konkar, A. "Nature of strained InAs three-dimensional island formation and distribution on GaAs(100)". *Applied Physics Letters* **64,** 2727–2729 (1994) (pg. 10).

99. Garcia, J. M. *et al.* "Intermixing and shape changes during the formation of InAs self-assembled quantum dots". *Applied Physics Letters* **71,** 2014–2016 (1997) (pg. 10).

100. Joyce, P. B., Krzyzewski, T. J., Bell, G. R., Joyce, B. A. & Jones, T. S. "Composition of InAs quantum dots on GaAs(001): Direct evidence for (In,Ga)As alloying". *Physical Review B* **58,** R15981–R15984 (1998) (pg. 10).

101. Ioffe Physico-Technical Institute. *Physical Properties of Semiconductors, http://www.ioffe.rssi.ru/SVA/NSM/Semicond/* (pg. 11).

102. Finley, J. J. *et al.* "Fine structure of charged and neutral excitons in InAs-Al0.6Ga0.4As quantum dots". *Physical Review B* **66,** 153316 (2002) (pg. 11).

103. Högele, A. *et al.* "Voltage-controlled optics of a quantum dot". *Physical Review Letters* **93,** 19–22 (2004) (pg. 11).

104. Kavokin, K. V. "Fine structure of the quantum-dot trion". *physica status solidi (a)* **195,** 592–595 (2003) (pg. 15).

105. Bracker, A. S., Gammon, D. & Korenev, V. L. "Fine structure and optical pumping of spins in individual semiconductor quantum dots". *Semiconductor Science and Technology* **23,** 114004 (2008) (pg. 15).

106. Igarashi, Y. *et al.* "Spin dynamics of excited trion states in a single InAs quantum dot". *Physical Review B* **81,** 245304 (2010) (pg. 15).

107. Finley, J. J. *et al.* "Charged and neutral exciton complexes in individual self-assembled In(Ga)As quantum dots". *Physical Review B* **63,** 073307 (2001) (pg. 15).

108. Akimov, I. A., Hundt, A., Flissikowski, T. & Henneberger, F. "Fine structure of the trion triplet state in a single self-assembled semiconductor quantum dot". *Applied Physics Letters* **81,** 4730 (2002) (pg. 15, 26).

109. Urbaszek, B. *et al.* "Fine Structure of Highly Charged Excitons in Semiconductor Quantum Dots". *Physical Review Letters* **90,** 247403 (2003) (pg. 15).

110. Van Kesteren, H. W., Cosman, E. C., van der Poel, W. A. J. A. & Foxon, C. T. "Fine structure of excitons in type-II GaAs/AlAs quantum wells". *Physical Review B* **41,** 5283–5292 (1990) (pg. 17).

111. Blackwood, E., Snelling, M. J., Harley, R. T., Andrews, S. R. & Foxon, C. T. B. "Exchange interaction of excitons in GaAs heterostructures". *Physical Review B* **50,** 14246–14254 (1994) (pg. 17).

112. Abragam, A. *The Principles of Nuclear Magnetism* (Oxford University Press, London, 1961) (pg. 18, 22).

113. Paget, D., Lampel, G., Sapoval, B. & Safarov, V. I. "Low field electron-nuclear spin coupling in gallium arsenide under optical pumping conditions". *Physical Review B* **15** (1977) (pg. 18, 20).

114. Bulutay, C. "Quadrupolar spectra of nuclear spins in strained In xGa 1-xAs quantum dots". *Physical Review B - Condensed Matter and Materials Physics* **85,** 115313 (2012) (pg. 18).

115. Bulutay, C., Chekhovich, E. A. & Tartakovskii, A. I. "Nuclear magnetic resonance inverse spectra of InGaAs quantum dots: Atomistic level structural information". *Physical Review B* **90,** 205425 (2014) (pg. 18, 23).

116. Slichter, C. P. *Principles of Magnetic Resonance* (Springer Berlin Heidelberg, Berlin, Heidelberg, 1990) (pg. 18).

117. Maletinsky, P., Kroner, M. & Imamoglu, A. "Breakdown of the nuclear-spin-temperature approach in quantum-dot demagnetization experiments". *Nature Physics* **5,** 407–411 (2009) (pg. 19).

118. Paget, D., Amand, T. & Korb, J. P. "Light-induced nuclear quadrupolar relaxation in semiconductors". *Physical Review B - Condensed Matter and Materials Physics* **77,** 1–12 (2008) (pg. 19).

119. Chekhovich, E. A. *et al.* "Dynamics of optically induced nuclear spin polarization in individual InP/Ga_{x}In_{1-x}P quantum dots". *Physical Review B* **81** (2010) (pg. 19, 22, 31, 44).

120. Marcinkevičius, S., Gaarder, A. & Leon, R. "Rapid carrier relaxation by phonon emission in In0.6Ga0.4As/GaAs quantum dots". *Physical Review B* **64,** 115307 (2001) (pg. 19).

121. Sun, K. W., Kechiantz, A., Lee, B. C. & Lee, C. P. "Ultrafast carrier capture and relaxation in modulation-doped InAs quantum dots". *Applied Physics Letters* **88,** 163117 (2006) (pg. 19).

122. Baylac, B. *et al.* "Hole spin relaxation in intrinsic quantum wells". *Surface Science* **326,** 161–166 (1995) (pg. 19).

123. Ohno, Y., Terauchi, R., Adachi, T., Matsukura, F. & Ohno, H. "Spin Relaxation in GaAs(110) Quantum Wells". *Physical Review Letters* **83,** 4196–4199 (1999) (pg. 19).

124. Wu, M. W., Jiang, J. H. & Weng, M. Q. "Spin dynamics in semiconductors". *Physics Reports* **493,** 61–236 (2010) (pg. 19).

125. Coish, W. A. & Baugh, J. "Nuclear spins in nanostructures". *Physica Status Solidi (B) Basic Research* **246,** 2203–2215 (2009) (pg. 19).

126. Latta, C., Srivastava, A. & Imamoglu, A. "Hyperfine Interaction-Dominated Dynamics of Nuclear Spins in Self-Assembled InGaAs Quantum Dots". *Physical Review Letters* **107,** 167401 (2011) (pg. 20).

127. Dyakanov, M. I. *Springer Series in Solid-state Sciences Vol. 157 Spin Physics in Semiconductors* (Springer-Verlag, Berlin, 2008) (pg. 23, 44).

128. Chekhovich, E. A. *et al.* "Structural analysis of strained quantum dots using nuclear magnetic resonance." *Nature nanotechnology* **7,** 646–50 (2012) (pg. 23).

129. Chekhovich, E. A., Krysa, A. B., Skolnick, M. S. & Tartakovskii, A. I. "Light-polarization-independent nuclear spin alignment in a quantum dot". *Physical Review B* **83,** 1–6 (2011) (pg. 24).

130. Kumagai, N. *et al.* "Suppression of indefinite peaks in InAs/GaAs quantum dot spectrum by low temperature capping in the indium-flush method". *Physica E: Low-dimensional Systems and Nanostructures* **42,** 2753–2756 (2010) (pg. 24).

131. Harbord, E. *et al.* "Enhancement of Valence Band Mixing in Individual InAs/GaAs Quantum Dots by Rapid Thermal Annealing". *Japanese Journal of Applied Physics* **52,** 125001 (2013) (pg. 24).

132. Tartakovskii, A. I. *et al.* "Dynamics of Coherent and Incoherent Spin Polarizations in Ensembles of Quantum Dots". *Physical Review Letters* **93,** 057401 (2004) (pg. 26).

133. Cortez, S. *et al.* "Optically Driven Spin Memory in n-Doped InAs-GaAs Quantum Dots". *Physical Review Letters* **89,** 207401 (2002) (pg. 26).

134. Ware, M. E. *et al.* "Polarized Fine Structure in the Photoluminescence Excitation Spectrum of a Negatively Charged Quantum Dot". *Physical Review Letters* **95,** 177403 (2005) (pg. 26).

135. Sallen, G. *et al.* "Nuclear magnetization in gallium arsenide quantum dots at zero magnetic field." *Nature communications* **5,** 3268 (2014) (pg. 27, 29).

136. Bayer, M. *et al.* "Inhibition and enhancement of the spontaneous emission of quantum dots in structured microresonators". *Physical Review Letters* **86,** 3168–3171 (2001) (pg. 30, 32, 41, 47).

137. Winger, M *et al.* "Explanation of photon correlations in the far-off-resonance optical emission from a quantum-dot-cavity system". *Physical Review Letters* **103,** 11–14 (2009) (pg. 30).

138. Raymond, S., Guo, X., Merz, J. & Fafard, S. "Excited-state radiative lifetimes in self-assembled quantum dots obtained from state-filling spectroscopy". *Physical Review B* **59,** 7624–7631 (1999) (pg. 30).

139. Raymond, S. *et al.* "State filling and time-resolved photoluminescence of excited states in \ce{In$_x$Ga$_{1-x}$As/GaAs} self-assembled quantum dots". *Physical Review B* **54,** 548–554 (1996) (pg. 30).

140. Kleppner, D. "Inhibited spontaneous emission". *Physical Review Letters* **47,** 233–236 (1981) (pg. 38).

141. Takagi, H. *et al.* "High Q H1 photonic crystal nanocavities with efficient vertical emission". *Optics Express* **20,** 28292 (2012) (pg. 38).

142. Puebla, J. *et al.* "Dynamic nuclear polarization in InGaAs/GaAs and GaAs/AlGaAs quantum dots under nonresonant ultralow-power optical excitation". *Physical Review B* **88,** 045306 (2013) (pg. 40).

143. Englund, D. *et al.* "Controlling the Spontaneous Emission Rate of Single Quantum Dots in a Two-Dimensional Photonic Crystal". *Physical Review Letters* **95,** 013904 (2005) (pg. 41, 47).

144. Chang, W. H. *et al.* "Efficient single-photon sources based on low-density quantum dots in photonic-crystal nanocavities". *Physical Review Letters* **96,** 117401 (2006) (pg. 41, 47).

145. Wang, Q., Stobbe, S. & Lodahl, P. "Mapping the Local Density of Optical States of a Photonic Crystal with Single Quantum Dots". *Physical Review Letters* **107,** 167404 (2011) (pg. 41).

146. Khanikaev, A. B. "Optical physics: On-chip synthetic magnetic field". *Nature Photonics* **7,** 941–943 (2013) (pg. 47).

147. Lodahl, P., Mahmoodian, S. & Stobbe, S. "Interfacing single photons and single quantum dots with photonic nanostructures". *Reviews of Modern Physics* **87,** 347–400 (2015) (pg. 47).

148. Luxmoore, I. J. *et al.* "Optical control of the emission direction of a quantum dot". *Applied Physics Letters* **103,** 2013–2016 (2013) (pg. 49).

149. Söllner, I. *et al.* "Deterministic photon-emitter coupling in chiral photonic circuits supplementary information". *Nature nanotechnology* **10,** 1406.4295 (2015) (pg. 49).

150. Coles, R. J. *et al.* "Chirality of nanophotonic waveguide with embedded quantum emitter for unidirectional spin transfer." *Nature communications* **7,** 11183 (2016) (pg. 49).

151. Sun, S., Kim, H., Solomon, G. S. & Waks, E. "Ultra-fast quantum interface between a solid-state spin and a photon". *Nature Nanotechnology* **11,** 46 (2016) (pg. 49).

152. Duan, L. M. & Kimble, H. J. "Scalable photonic quantum computation through cavity-assisted interactions". *Physical Review Letters* **92,** 127902–1 (2004) (pg. 49).

153. Sweeney, T. M. *et al.* "Cavity-stimulated Raman emission from a single quantum dot spin". *Nature Photonics* **8,** 442–447 (2014) (pg. 49).

154. Jarlov, C. *et al.* "Exciton dynamics in a site-controlled quantum dot coupled to a photonic crystal cavity". *Applied Physics Letters* **107** (2015) (pg. 49).

155. Kuruma, K. *et al.* "Position dependent optical coupling between single quantum dots and photonic crystal nanocavities". *Applied Physics Letters* **109,** 071110 (2016) (pg. 49).

156. Hoang, T. B. *et al.* "Ultrafast spontaneous emission source using plasmonic nanoantennas." *Nature communications* **6,** 7788 (2015) (pg. 50).

157. Makhonin, M. N. *et al.* "Fast control of nuclear spin polarization in an optically pumped single quantum dot." *Nature materials* **10,** 844–8 (2011) (pg. 52).

158. Waeber, A. M. *et al.* "Few-second-long correlation times in a quantum dot nuclear spin bath probed by frequency-comb nuclear magnetic resonance spectroscopy". *Nature Physics* **12,** 688–693 (2016) (pg. 53).

159. Quinteiro, G. F. & Tamborenea, P. I. "Electronic transitions in disk-shaped quantum dots induced by twisted light". *Physical Review B* **79,** 1–7 (2009) (pg. 53).

160. Quinteiro, G. F. & Kuhn, T. "Light-hole transitions in quantum dots: Realizing full control by highly focused optical-vortex beams". *Physical Review B* **90,** 1–9 (2014) (pg. 53).

161. Lezec, H. J. *et al.* "Beaming light from a subwavelength aperture." *Science (New York, N.Y.)* **297,** 820–822 (2002) (pg. 53).

List of Publications

International Journals

- C. F. Fong, Y. Ota, E. Harbord, S. Iwamoto and Y. Arakawa, "P-shell carriers assisted dynamic nuclear spin polarization in single quantum dots at zero external magnetic field", Phys. Rev. B 93, 125306 (2016)
- C. F. Fong, Y. Ota, S. Iwamoto and Y. Arakawa, "Manipulation of dynamic nuclear spin polarization in single quantum dots by photonic environment engineering", Phys. Rev. B 95, 245423 (2017)

International Conferences and Workshops

- C. F. Fong, Y. Ota, E. Harbord, S. Iwamoto and Y. Arakawa, "Dynamic Nuclear Spin Polarization by P-shell Electrons in Single Quantum Dots at Zero External Magnetic Field", International Nano Optoelectronics Workshop (iNOW) 2015, poster ThP5, August 3-7th, Tokyo, Japan (Student Poster Award)
- C. F. Fong, Y. Ota, E. Harbord, S. Iwamoto and Y. Arakawa, "Dynamic Nuclear Spin Polarization by P-shell Carriers in Single Quantum Dots", 17th International Conference on Modulated Semiconductor Structures, poster Tu-PM-8, July 26th-31st, 2015, Sendai, Japan
- C. F. Fong, Y. Ota, , S. Iwamoto and Y. Arakawa, "Modification of dynamic nuclear spin polarization in single quantum dots by photonic crystals", The 24th Congress of the International Commission for Optics (ICO-24), oral Th1E-06, August 21st-25th, 2017, Tokyo, Japan (OSA/SPIE Student Paper Award)

Domestic Conferences

- C. F. Fong, Y. Ota, E. Harbord, S. Iwamoto and Y. Arakawa, "Measurement of Nuclear Spin Build-up Time in Single InAs/GaAs Quantum Dots by Modulated Circularly Polarized Excitation", 75^{th} Autumn Meet, Japan Society of Applied Physics and Related Societies, 18a-A27-8, Hokkaido University, Hokkaido.

- C. F. Fong, Y. Ota, E. Harbord, S. Iwamoto and Y. Arakawa, "Dynamic Nuclear Spin Polarization in the Presence of Multiple Excitonic Complexes in Single InAs/GaAs Quantum Dots at Zero Applied Magnetic Field", 62^{nd} Spring Meet, Japan Society of Applied Physics and Related Societies, Tokai University, Tokyo.

- C. F. Fong, Y. Ota, S. Iwamoto and Y. Arakawa, "Modulation of Dynamic Nuclear Spin Polarization in Single InAs/GaAs Quantum Dots by Photonic Bandgap Effect", 63^{rd} Spring Meet, Japan Society of Applied Physics and Related Societies, Tokyo Inst. Of Tech., Ookayama, Tokyo.

- C. F. Fong, E. A. Chekhovich, A. Ulhaq, M. S. Skolnick, Y. Ota, S. Iwamoto, Y. Arakawa, "Analysis on Optically-detected Electron Spin Resonance in Single Self-Assembled Quantum Dots", 64^{th} Spring Meet, Japan Society of Applied Physics and Related Societies, Pacifico Yokohama, Yokohama.

List of Figures

List of Tables